CJC Chinese Journal of Chemistry 中国化学 - An International Journal

For submission: https://mc.manuscriptcentral.com/cjoc
For published articles: https://onlinelibrary.wiley.com/journal/16147065

Concise Report

Cite this paper: *Chin. J. Chem.* **2023**, *41*, 2453—2468. **DOI: 10.1002/cjoc.202300166**

Guaiane-type Sesquiterpenoid Dimers from *Artemisia zhongdianensis* and Antihepatoma Carcinoma Activity *via* the p38MAPK Pathway

Wei Dong,[a,b] Wen-Jing Ma,[a,b] Yun-Bao Ma,[a] Feng-Jiao Li,[a,b] Tian-Ze Li,[a] Yong-Cui Wang,[a] Xiao-Feng He,[a] Chang-An Geng,[a] Xue-Mei Zhang,[a] and Ji-Jun Chen*[,a,b]

[a] *State Key Laboratory of Phytochemistry and Plant Resources in West China, Kunming Institute of Botany, Chinese Academy of Sciences, Kunming, Yunnan 650201, China*
[b] *University of Chinese Academy of Sciences, Beijing 100049, China*

Keywords

Artemzhongdianolides B1—B17 | *Artemisia zhongdianensis* | Guaiane-type sesquiterpenoid dimers | Antihepatoma activity | p38MAPK pathway | Cancer | NMR spectroscopy | X-ray diffraction

Comprehensive Summary

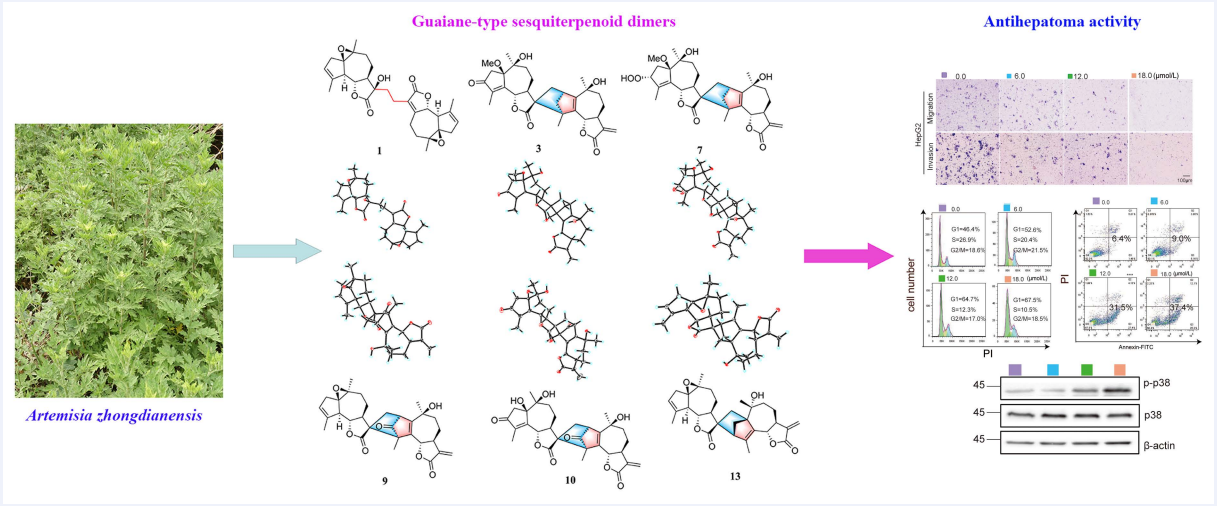

17 new guaiane-type sesquiterpenoid dimers (GSDs), artemzhongdianolides B1—B17 (**1**—**17**), were isolated from *Artemisia zhongdianensis* under the guidance of bioassay, and elucidated by spectral analyses (HRESIMS, 1D and 2D NMR, IR, ECD). The absolute configuration of compounds **1**, **3**, **7**, **9**, **10**, and **13** was determined by single-crystal X-ray diffraction analyses. Structurally, artemzhongdianolides B1 (**1**) and B2 (**2**) were the first example of the GSDs fused *via* a C-13/C-13' single bond, and artemzhongdianolides B3—B17 were [4 + 2] Diels–Alder adducts of two monomeric guaianolides. Most of the compounds showed antihepatoma cytotoxicity with IC_{50} values ranging from 9.9 to 170.1 μmol/L. Importantly, artemzhongdianolide B9 (**9**) was the most active one against three hepatoma cell lines with IC_{50} values of 13.1 μmol/L (HepG2), 19.5 μmol/L (Huh7), and 19.5 μmol/L (SK-Hep-1), and dose-dependently inhibited cell migration and invasion, induced G1 cell cycle arrest and cell apoptosis in HepG2 cells. Compound **9** might suppress HepG2 cells *via* affecting the p38MAPK signaling pathway suggested by machine learning approach, and significantly upregulated expression of phosphorylated p38 validated by Western blot assay.

*E-mail: chenjj@mail.kib.ac.cn

Background and Originality Content

Hepatocellular carcinoma (HCC) accounting for nearly 90% of primary liver cancer represents one of the most lethal and prevalent human cancers.[1] The incidence of HCC has nearly doubled over the past decade, making it the third-leading cause of cancer-related death worldwide.[2] Currently, four synthetic drugs (sorafenib, regorafenib, lenvatinib and cabozantinib) and three monoclonal antibody drugs (nivolumab, pembrolizumab and ramucirumab) have been approved for the treatment of HCC since 2007.[3] Whereas, those drugs remain modest and complex molecular pathogenesis of HCC and still need the investigation of novel chemical agents. Natural resources are concluded as the valuable repository of novel bioactive entities. In the last 30 years, about 50% of newly approved small-molecule drugs is from natural products, and most of them have been applied to treat cancers.[4]

Some plants of the genus *Artemisia* (the family Asteraceae) have been used as folk medicines to prevent or cure various diseases. As characteristic components of the genus *Artemisia*, sesquiterpenoid dimers have attracted extensive attention from chemists due to their novel structural architectures. Structurally, these sesquiterpenoid dimers are formed by two homo- or hetero-sesquiterpenoid monomers *via* Diels–Alder reaction, [2 + 2] cycloaddition, esterification, and so on.[5-6] Intriguingly, some sesquiterpenoid dimers exhibited remarkable cytotoxic activity in MCF-7, HepG2 and A549 cancer cell lines. For instance, artemiolides A—D, four sesquiterpenoid dimers from *A. sylvatica*, showed farnesyl protein transferase inhibitory activity with IC_{50} values of 0.7—1.8 μmol/L.[7] Artemisian B from *A. argyi* demonstrated significant cytotoxic effects with an IC_{50} value of 3.2 μmol/L by inducing G2/M cell cycle arrest and cell apoptosis in MDA-MB-468 cells.[8] Although the cytotoxic activities and preliminary mechanism of sesquiterpenoid dimers had been studied, diverse structures with different mechanism were worthy to investigate.

One of the mitogen-activated protein kinases, the p38 mitogen-activated protein kinases (p38MAPK), has been proven to be involved in a wide range of complex biologic processes, such as cell proliferation, differentiation, migration, and invasion.[9] The tumor suppressor potential of this signaling pathway is an interesting topic, and p38MAPK represents a potential target for cancer treatment. Recent studies indicated that p38 was significantly downregulated in hepatocellular carcinoma tumors.[10] Furthermore, telekin from the Chinese herb *Carpesium divaricatum* suppressed hepatocellular carcinoma cells *in vitro* by inducing G2/M phase arrest *via* activating the p38MAPK pathway.[11] Intriguingly, experimental evidences supported that upregulating phospho-p38 expression could revert sorafenib resistance in HCC cells.[12] Thus, the discovery of novel molecules acting on the p38 signaling pathway may offer another choice for the development of new antihepatoma drugs.

Machine learning is a subfield of artificial intelligence, and has been successfully applied in natural product chemistry and pharmacology, to predict compound–protein interactions and signaling pathway.[13] This predictive approach combined with experimental validation has become an important strategy in drug discovery.

Our previous investigation on *A. eriopoda* gave rise to 36 novel sesquiterpenoid dimers, and artemeriopodin G7 could inhibit cell migration and invasion, induce G2/M cell cycle arrest and apoptosis, upregulate PDGFRA expression in HepG2 cells, and suppress the activity of AKT/STAT signaling pathway;[14] artemeriopolide A from *A. eriopoda* and artemidubolide D from *A. dubia* induced G0/G1 cell cycle arrest and apoptosis;[15-16] 50 guaianolide dimers were isolated from *A. atrovirens* and *A. princeps*. Lavandiolide H and artemiprinolide A displayed obvious inhibition against three hepatoma cell lines, which suggested that they dose-dependently inhibited cell migration and invasion, induced G2/M cell cycle arrest and cell apoptosis in HepG2 cells.[5,17-19] Inspired by their obvious antihepatoma activity and structural features, lavandiolides H—K and artematrolide F had been successfully synthesized *via* the biomimetic Diels-Alder reaction.[20]

In our previous study, 21 new GSDs, artemzhongdianolides A1—A21 with antihepatic fibrosis activity were isolated from *A. zhongdianensis*.[21] Further assay suggested that fractions C and D form *A. zhongdianensis* showed remarkable antihepatoma inhibition of 75.9%, and 81.7% at 100.0 μg/mL against HepG2 cells. As a result, 17 new GSDs, artemzhongdianolides B1—B17 (**1**—**17**), were isolated from active fractions, and their structures were assigned *via* spectral analyses (HRESIMS, 1D and 2D NMR, IR, ECD) and X-ray diffraction. Structurally, artemzhongdianolides B1 (**1**) and B2 (**2**) were the first example of GSDs fused by a C-13/C-13' single bond. Compounds **3**—**9**, **13**, and **15** showed cytotoxicity against three hepatoma cell lines with IC_{50} values ranging from 9.9 to 140.3 μmol/L (HepG2), 18.6 to 77.5 μmol/L (Huh7), and 17.9 to 170.1 μmol/L (SK-Hep-1). Importantly, compound **9** was the most active one with IC_{50} values of 13.1 μmol/L (HepG2), 19.5 μmol/L (Huh7), and 19.5 μmol/L (SK-Hep-1), respectively. Thus, artemzhongdianolide B9 (**9**) was further investigated to explore the molecular mechanism against HCC. Machine learning approach was introduced to predict the targets of compound **9**. The mechanism of compound **9** in HepG2 cells was conducted by Transwell, Flow cytometer, and Western blot assays. Herein, the details of the isolation, structural elucidation, cytotoxic activities, and preliminary mechanism are reported.

Results and Discussion

Artemzhongdianolide B1 (**1**) was obtained as colorless monoclinic crystals with a molecular formula of $C_{30}H_{36}O_7$ as inferred from (+)-HRESIMS ion at *m/z* 509.2526 $[M + H]^+$ (calcd. 509.2534), suggesting 13 degrees of unsaturation. Its IR spectrum displayed characteristic absorption bands assignable to hydroxy (3523, 3436 cm^{-1}), ester carbonyl (1766, 1736 cm^{-1}), and olefinic (1661 cm^{-1}) functional groups. The ^1H NMR data (Table 1) of compound **1** exhibited four singlet methyls at δ_H 1.30 (3H, s), 1.33 (3H, s), 1.90 (3H, s), and 1.92 (3H, s), two oxygenated methines at δ_H 4.30 (1H, dd, *J* = 10.2, 10.2 Hz) and 4.69 (1H, d, *J* = 10.8 Hz), and two olefinic protons at δ_H 5.58 (1H, br s) and 5.62 (1H, br s). Its ^{13}C NMR and DEPT spectrum (Table 4) revealed the presence of 30 carbons classified as four methyls, eight methylenes, seven methines, 11 nonprotonated carbons. Among these carbons, two ester carbonyls at δ_C 177.0 and 173.9, and six olefinic carbons at δ_C 165.2, 141.5, 141.3, 126.5, 126.3, and 125.7 were easily recognized in the deshielded region. The evidence mentioned above suggested that compound **1** was a sesquiterpenoid dimer.

The planar structure of artemzhongdianolide B1 involving units A and B was mainly accomplished by analyzing the 2D NMR data (Figure 2). ^1H–^1H COSY spectrum revealed five isolated spin-coupling systems of H_2-2/H-3, H-5/H-6, H_2-8/H_2-9, H_2-2'/H-3', and H-5'/H-6'/H-7'/H_2-8'/H_2-9'. The HMBC spectrum showed correlations from H_2-13 to C-7, C-11, and C-12, from H_3-14 to C-1, C-9, and C-10, from H_3-15 to C-3, C-4, and C-5, and from H-6 to C-7, and C-11 in unit A; and correlations from H_3-14' to C-1', C-9', and C-10', from H_3-15' to C-3', C-4', and C-5', from H-6' to C-4', and C-11', and from H_2-13' to C-7', C-11', and C-12' in unit B. From the above analyses, both units A and B were deduced as guaianolide-like moieties. The linkage of units A and B through C—C single bond of C-13—C-13' was established by the key ^1H–^1H COSY correlations of H_2-13/H_2-13' and HMBC correlations of H_2-13 with C-11', of H_2-13' with C-11.

The relative configuration of **1** was determined by interpretation of ROESY spectrum (Figure 3) and coupling constants. With the fact that H-7 of guaiane-type sesquiterpenoids typically maintained the α-orientated,[22-23] the large coupling constants of

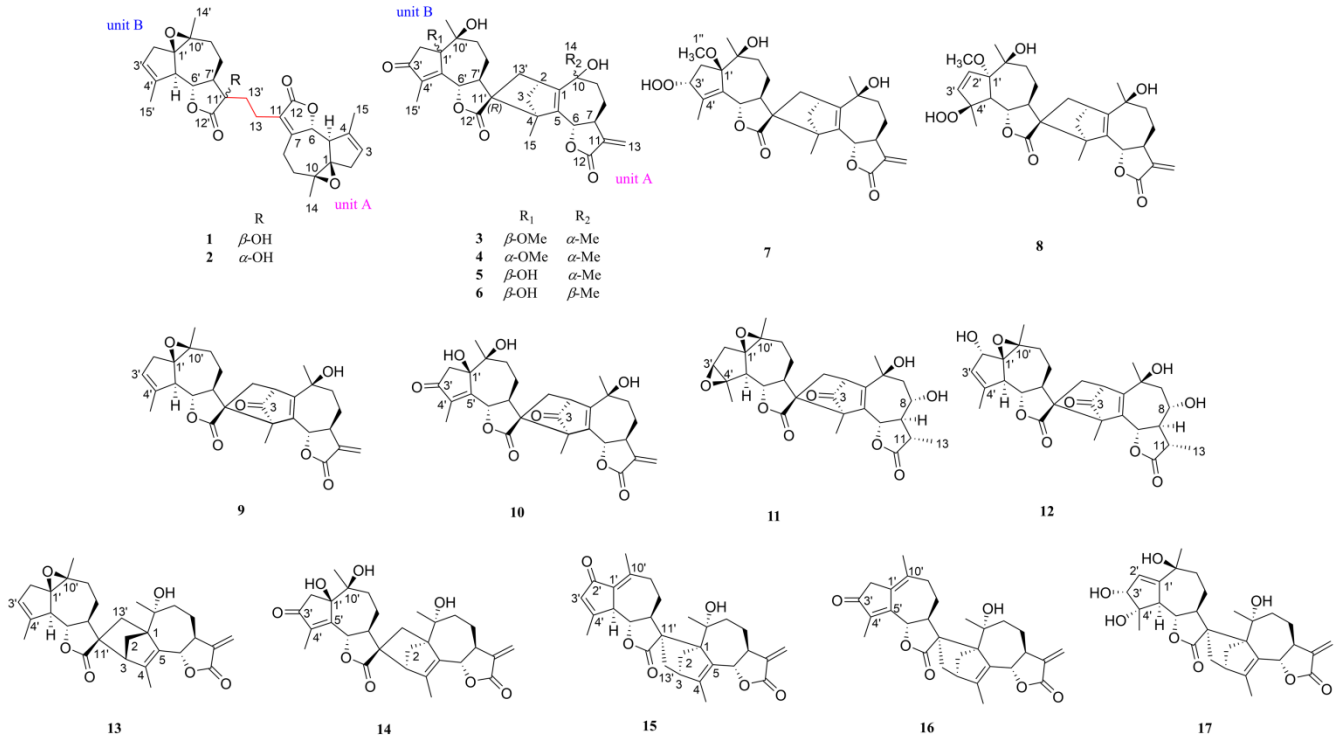

Figure 1 Chemical structures of artemzhongdianolides B1—B17 (**1**—**17**).

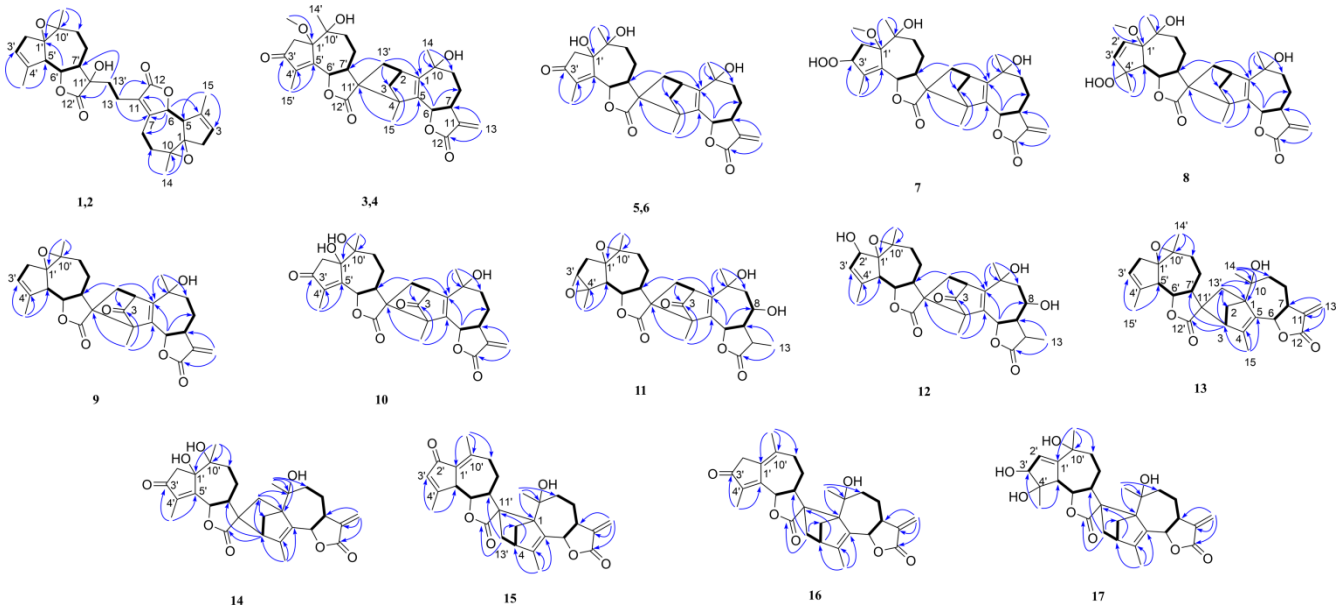

Figure 2 ^{1}H–^{1}H COSY (—) and key HMBC (→) correlations of compounds **1**—**17**.

H-5'/H-6' and H-6'/H-7' ($J_{5',6'}$ = $J_{6',7'}$ = 10.2 Hz) revealed that H-6' was *β*-orientated, H-5' and H-7' were *α*-orientated. Furthermore, unit A was also a guaiane-type sesquiterpenoid to support the *α*-orientation of H-5 and the *β*-orientation of H-6. The ROESY correlations of H-5/H_3-14 and H-5'/H_3-14' assigned their *α*-orientation. Similarly, OH-11' was assigned as *β*-orientation by the ROESY correlations of H-6'/OH-11'. To establish its absolute configuration, suitable crystals of compound **1** were obtained from an optimized solvent system (MeOH–CH_2Cl_2, 2:98, *V*/*V*), which facilitated the single-crystal X-ray diffraction experiment with Cu Kα radiation [Flack parameter of 0.04(6)] (Figure 4). Consequently, the absolute configuration of compound **1** was unambiguously determined as (1*R*,5*R*,6*R*,10*S*,1'*R*,5'*R*,6'*S*,7'*R*,10'*S*,11'*R*).

Artemzhongdianolide B2 (**2**) had the same molecular formula of $C_{30}H_{36}O_7$ with compound **1** by the (+)-HRESIMS ion at *m*/*z* 509.2530 $[M + H]^+$ (calcd. 509.2534). Analyses of the 1D and 2D NMR data (Tables 1 and 4) suggested that compound **2** had the same planar structure with compound **1**. By comparing with compound **1**, the chemical shifts of C-7', C-11', and C-13' in compound **2** were significantly shielded, changing from δ_C 53.8, 76.2, and 33.6 in compound **1** to 58.4, 76.6, and 30.7 in compound **2**, suggesting the varied stereochemistry at C-11'. In the ROESY spectrum (Figure 3), the correlation of H-6'/H-13'a was readily detected, supporting the *β*-orientation of H_2-13'. The relative configuration of unit A was confirmed by the ROESY experiment, which was the same as that of compound **1**. By means of electronic circular dichroism (ECD) calculation (Figure 5), the absolute configuration of **2** was assigned as (1*R*,5*R*,6*R*,10*S*,1'*R*,5'*R*,6'*S*,7'*R*,10'*S*,11'*S*).

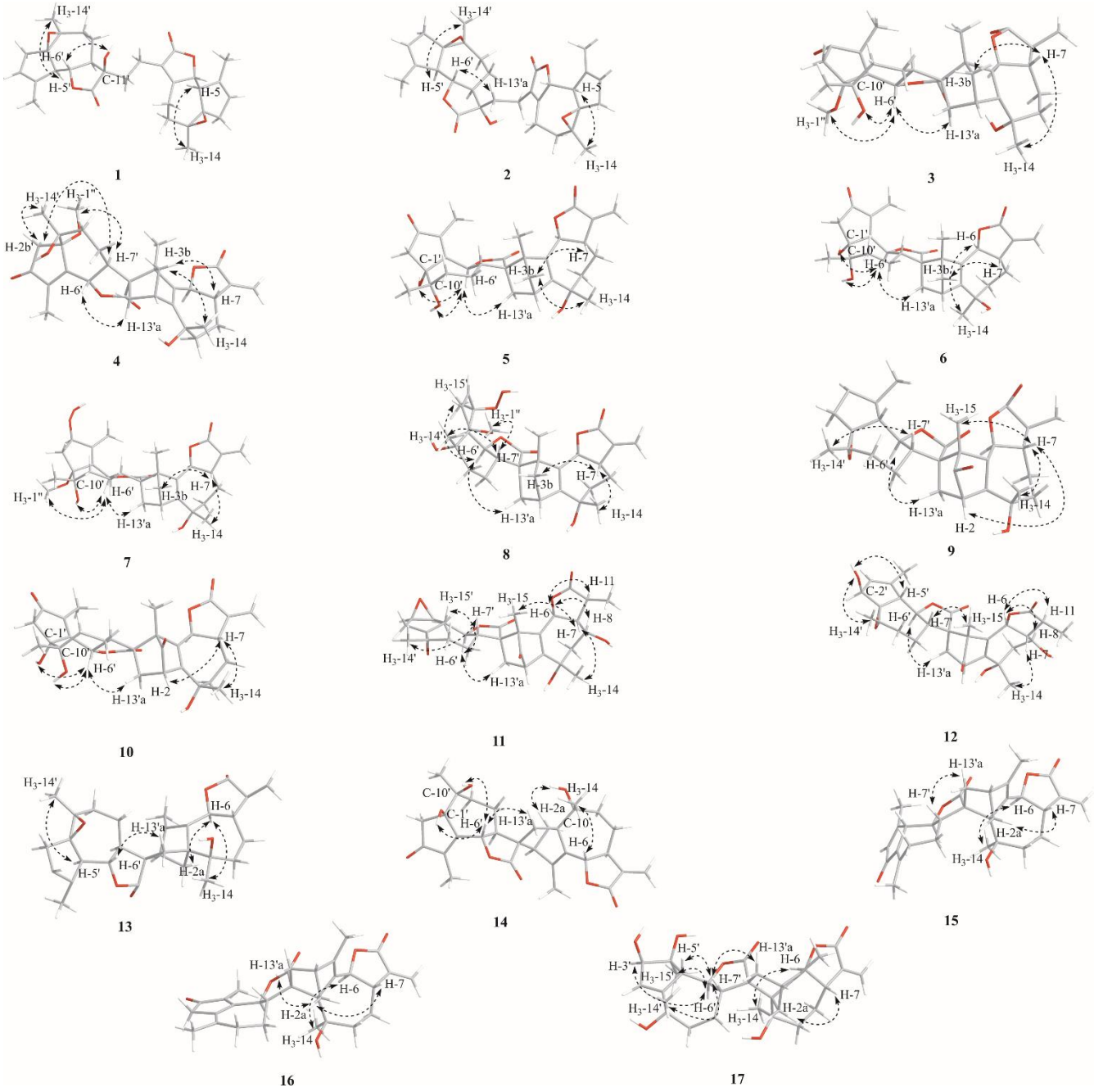

Figure 3 Key ROESY correlations of compounds **1**—**17**.

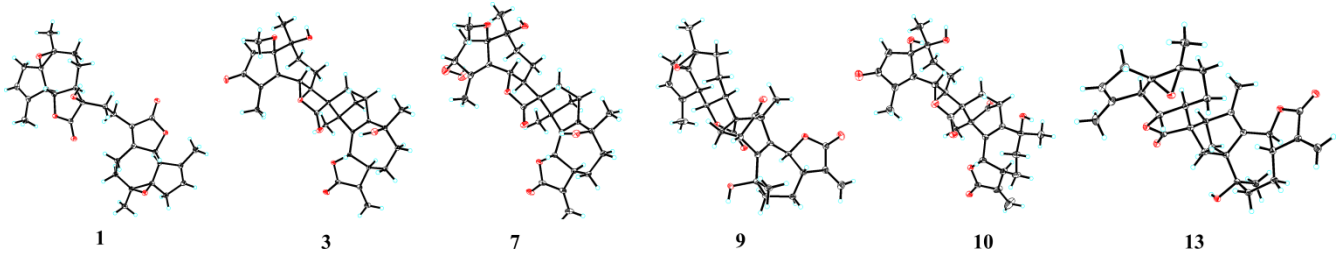

Figure 4 The X-ray ORTEP drawings of compounds **1**, **3**, **7**, **9**, **10**, and **13**.

Artemzhongdianolide B3 (**3**) was obtained as colorless orthorhombic crystals with a molecular formula of $C_{31}H_{38}O_8$ from the $[M–H]^-$ ion at *m/z* 537.2499 (calcd. 537.2494) in the (–)-HRESIMS data. The presence of hydroxy (3442 cm^{-1}), carbonyl (1765, and 1713 cm^{-1}), and olefinic (1634 cm^{-1}) groups was suggested by the IR spectrum. The ^1H NMR spectrum (Table 1) of compound **3** displayed five methyl groups at δ_H 1.26 (3H, s), 1.42 (3H, s), 1.44 (3H, s), 1.95 (3H, s), and 3.12 (3H, s), two oxygenated methine signals at δ_H 5.08 (1H, d, *J* = 10.8 Hz) and 5.55 (1H, d, *J* = 10.2 Hz), and two olefinic protons at δ_H 5,45 (1H, d, *J* = 3.0 Hz), 6.17 (1H, d, *J* = 3.0 Hz). The ^{13}C NMR and DEPT spectrum (Table 4) displayed the presence of 31 carbon resonances, including three pair of olefinic carbons (δ_C 151.9 and 144.2, 140.1 and 119.2, 162.4 and 141,2), two lactone carbonyl carbons (δ_C 170.2 and 180.2), and one carbonyl carbon (δ_C 204.4). Overall, compound **3** was also deduced as a dimer derived from two different guaiane units.

Table 1 ^{1}H NMR data (600 MHz) for compounds **1**—**6** (*J* in Hz)

No.	**1**[a]	**2**[a]	**3**[b]	**4**[b]	**5**[b]	**6**[b]
2	2.77 m	2.77 m	3.09 br s	3.22 br s	3.08 br s	3.22 br s
	2.16 m	2.16 m				
3	5.62 br s	5.61 br s	1.46 d (9.6)	1.64 m	1.46 m	1.49 d (8.4)
			1.36 d (9.6)	1.42 m	1.36 m	1.40 [c]
5	2.67 d (12.0)	2.66 d (11.4)				
6	4.69 d (10.8)	4.68 d (10.8)	5.55 d (10.2)	5.38 d (10.2)	5.52 d (10.2)	5.40 d (10.2)
7			2.85 m	2.92 m	2.84 m	2.93 m
8	2.74 m	2.71 m	2.16 m	2.31 m	2.16 m	2.32 m
	1.29 m	2.32 m	1.84 m	1.70 m	1.82 m	1.69 m
9	2.14 m	2.18 m	2.04 m	1.91 m	2.02 m	1.90 m
	2.06 m	2.16 m	1.82 m	1.89 m	1.81 m	1.88 m
13	2.44 m	2.55 m	6.17 d (3.0)	6.17 d (3.3)	6.17 d (3.3)	6.17 d (3.0)
	2.26 m	2.28 m	5.45 d (3.0)	5.46 d (3.3)	5.45 d (3.3)	5.46 d (3.0)
14	1.33 s	1.33 s	1.42 s	1.36 s	1.42 s	1.34 s
15	1.92 s	1.92 s	1.44 s	1.48 s	1.42 s	1.44 s
2'	2.08 m	2.79 m	2.48 d (18.6)	2.76 d (18.6)	2.49 br d (7.2)	2.51 br s
	2.81 m	2.08 m	2.31 d (18.6)	2.44 d (18.6)		
3'	5.58 br s	5.58 br s				
5'	2.95 d (10.2)	2.91 d (10.2)				
6'	4.30 dd (10.2, 10.2)	4.02 dd (10.5, 10.5)	5.08 d (10.8)	4.82 d (10.8)	5.18 d (10.8)	5.22 d (10.8)
7'	1.76 m	2.00 m	2.43 m	3.11 t (10.8)	2.38 m	2.42 m
8'	1.58 m	1.61 m	2.13 m	1.82 m	2.12 m	2.14 m
	1.57 m	1.42 m	1.57 m	1.67 m	1.55 m	1.60 [c]
9'	2.15 m	2.14 m	2.00 m	2.35 m	1.98 m	2.02 m
	2.13 m	2.02 m	1.52 m	1.65 m	1.52 m	1.54 [c]
13'	1.94 m	1.75 m	2.40 m	2.19 m	2.41 m	2.43 m
	1.83 m	1.71 m	1.54 m	1.49 m	1.58 m	1.42 m
14'	1.30 s	1.29 s	1.26 s	1.38 s	1.31 s	1.33 s
15'	1.90 s	1.89 s	1.95 s	1.93 s	1.86 s	1.90 s
1''			3.12 s (OCH_3)	3.06 s (OCH_3)		

[a] Data were recorded in acetone-d_6. [b] Data were recorded in $CDCl_3$. [c] "ol" is used to indicate overlapped signals, for which the coupling constants could not be read.

The structure of **3** was constructed on the basis of ^{1}H–^{1}H COSY and HMBC data (Figure 2). ^{1}H–^{1}H COSY spectrum revealed three isolated spin-coupling systems of H-6/H-7/H_2-8/H_2-9, H_2-13'/H-2/H-3, and H-6'/H-7'/H_2-8'/H_2-9'. The HMBC spectrum showed correlations from H_2-13 to C-7, C-11, and C-12, from H_3-14 to C-1, C-9, and C-10, and from H_3-15 to C-3, C-4, and C-5 in unit A; and correlations from H_3-14' to C-1', C-9', and C-10', from H_3-15' to C-3', C-4', and C-5', and from H-6' to C-4', C-8', and C-11' in unit B. On the basis of the above data, the monomeric A and B units were deduced as two different guaiane-type sesquiterpenoid. The key HMBC correlations of H-13' with C-1, C-2, and C-3, of H_3-15 with C-11', as well as ^{1}H–^{1}H COSY correlation of H_2-13' with H-2, indicated units A and B are linked *via* C-2—C-13' and C-4—C-11', with the bicyclic [2.2.1]hept-2-ene ring presumably formed through a [4+2] Diels–Alder cyclo-addition reaction.

The ROESY spectrum and the coupling constants were employed to determine the relative configuration of **3**. The large coupling constant between H-6 and H-7 ($J_{6,7}$ = 10.2 Hz) indicated H-6 and H-7 were in *anti*-axial configuration, and H-6 was assigned to be *β*-orientated. Similarly, the large coupling constant between H-6′ and H-7′ ($J_{6',7'}$ = 10.8 Hz) indicated H-6′ was *β*-orientated. In the ROESY spectrum, the cross peaks of H-6′/OH-10′/H_3-1′′, and H-6′/H-13′a indicated that OH-10′, CH_3-1′′ and CH_2-13′ were *β*-orientated, while the correlations of H-7 with H-3b and H_3-14 assigned the *α*-orientation of H_2-3 and H_3-14. The structure of compound **3** was confirmed through a single crystal X-ray diffraction experiment with Cu Kα radiation [Flack parameter of 0.04(3)], and the absolute stereochemistry was confirmed as (2*S*,4*S*,6*S*,7*S*,10*S*,1′*R*,6′*S*,7′*S*,10′*S*,11′*R*).

Artemzhongdianolide B4 (**4**) had the same molecular formula of $C_{31}H_{38}O_8$ with compound **3** by the (–)-HRESIMS ion at *m*/*z* 537.2497 $[M–H]^-$ (calcd. 537.2494). Analyses of the 1D and 2D NMR data (Tables 1 and 4) suggested that compound **4** had the same planar structure with compound **3**. By comparing with compound **3**, the chemical shifts of C-1', C-5', and C-10' were significantly shielded from δ_C 84.9, 162.4, and 73.6 in **3** to 88.4, 159.0, and 76.2 in **4**, suggesting the varied stereochemistry at C-1'. In the ROESY spectrum (Figure 3), the correlation of H-7'/H-1'' was readily detected, supporting the *α*-orientation of H-7' and H-1''. The relative configuration of unit A was confirmed by the ROESY experiment, which was the same as that of compound **3**. By means of ECD calculation (Figure 5), the absolute configuration of **4** was assigned as (2*S*,4*S*,6*S*,7*S*,10*S*,1'*S*,6'*S*,7'*S*,10'*S*,11'*R*).

Artemzhongdianolide B5 (**5**) was obtained as a white powder with a molecular formula of $C_{30}H_{36}O_8$ from the $[M + H]^+$ ion at *m*/*z* 525.2492 (calcd. 525.2483) in the (+)-HRESIMS data. The presence of hydroxy (3431 cm^{-1}), carbonyl (1765 and 1712 cm^{-1}), and olefinic (1644 cm^{-1}) groups was suggested by the IR spectrum. The ^{1}H NMR data and ^{13}C NMR (DEPT) data of compound **5** were similar to those of compound **3** except for the shielded shifts of C-1' (from δ_C 84.9 in **3** to 80.2 in **5**). Considering the difference of 14 Da (CH_2) between their molecular weights, a hydroxy instead of a methoxy group was present at C-1' in **5**. Analyses of their ROESY and ECD spectra (Figures 3 and 5) suggested **5** had the same absolute configuration as **3**. Thus, the structure of compound **5** was defined as (2*S*,4*S*,6*S*,7*S*,10*S*,1'*R*,6'*S*,7'*S*,10'*S*,11'*R*).

Table 2 ^{1}H NMR data (600 MHz) for compounds **7**—**12** (*J* in Hz)

No.	**7**[b]	**8**[b]	**9**[b]	**10**[a]	**11**[b]	**12**[a]
2	3.04 br s	3.06 br s	3.24 d (4.2)	3.30 m	3.20 d (3.0)	3.19 d (3.6)
3	1.43 m	1.46 m				
	1.32 m	1.32 m				
6	5.57 d (10.2)	5.47 d (10.2)	5.57 d (9.6)	5.54 d (10.2)	5.51 d (10.8)	5.48 d (10.8)
7	2.85 m	2.79 m	2.93 m	3.10 m	2.16 q (9.6)	2.22 m
8	2.14 m	2.13 m	2.19 m	2.28 m	4.24 m	4.22 m
	1.81 m	1.97 m	1.83 m	1.79 m		
9	2.02 m	2.03 m	2.13 m	2.61 m	2.28 dd (14.4, 4.2)	2.24 [c]
	1.84 m	1.77 m	1.86 m	1.81 m	1.85 m	1.94 m
11					2.54 m	2.62 m
13	6.16 d (3.3)	6.18 d (3.6)	6.19 d (3.3)	6.05 d (3.3)	1.40 d (7.2)	1.32 d (7.2)
	5.44 d (3.3)	5.47 d (3.6)	5.48 d (3.3)	5.50 d (3.3)		
14	1.41 s	1.42 s	1.43 s	1.45 s	1.53 s	1.53 s
15	1.44 s	1.50 s	1.38 s	1.32 s	1.34 s	1.26 s
2'	2.21 dd (15.0, 6.6)	5.84 d (6.0)	2.76 d (17.4)	2.57 d (18.0)	2.37 [c]	4.14 d (4.8)
	2.02 m		2.13 m	2.34 d (18.0)	1.89 [c]	
3'	4.97 t (6.3)	6.18 d (6.0)	5.57 [c]		3.32 br s	5.75 br s
5'		2.87 d (9.6)	1.84 [c]		2.39 d (10.2)	3.20 d (10.2)
6'	4.79 d (10.8)	4.54 dd (9.9, 9.9)	4.04 dd (10.2, 10.2)	5.40 d (10.8)	4.17 dd (10.2, 10.2)	3.92 dd (10.2, 10.2)
7'	2.36 td (11.4, 5.4)	2.77 m	2.83 br d (10.2)	2.45 td (10.8, 6.0)	1.81 m	1.96 m
8'	2.07 m	1.73 m	1.45 m	1.88 m	1.42 m	1.40 m
	1.45 m	1.56 m	1.23 m	1.35 m	1.18 m	1.18 m
9'	1.76 m	2.38 m	2.07 m	1.94 m	2.04 dd (15.0, 5.4)	2.07 m
	1.73 m	1.55 m	1.95 m	1.67 m	1.80 m	2.05 m
13'	2.41 dd (12.0, 3.6)	2.34 m	2.39 dd (12.6, 4.2)	2.11 m	2.37 m	2.38 dd (12.0, 3.6)
	1.49 m	1.49 m	1.62 m	1.81 m	1.60 m	1.73 d (12.6)
14'	1.24 s	1.29 s	1.32 s	1.26 s	1.26 s	1.46 s
15'	1.97 s	1.42 s	1.91 s	1.80 s	1.62 s	1.91 s
1''	3.13 s (OCH_3)	3.30 s (OCH_3)				

[a] Data were recorded in acetone-d_6. [b] Data were recorded in $CDCl_3$. [c] "ol" is used to indicate overlapped signals, for which the coupling constants could not be read.

Artemzhongdianolide B6 (**6**) had the same molecular formula of $C_{30}H_{36}O_8$ with compound **5** by the (–)-HRESIMS ion at *m*/*z* 523.2351 $[M–H]^-$ (calcd. 523.2337). Analyses of the 1D and 2D NMR data (Tables 1 and 4) suggested that compound **6** had the same planar structure with compound **5**. By comparing with **5**, the chemical shifts of C-1, C-9, and C-10 were significantly shielded from δ_C 151.9, 38.5, and 72.8 in **5** to 150.8, 40.0, and 73.5 in **6**, suggesting the varied stereochemistry at C-10. In the ROESY spectrum (Figure 3), the correlation of H-6/H_3-14 was readily detected, supporting the *β*-orientation of H-6 and CH_3-14, by which compound **6** was determined as the 10-epimer of compound **5**. By means of ECD calculation (Figure 5), the absolute configuration of **6** was assigned as (2*S*,4*S*,6*S*,7*S*,10*R*,1'*R*,6'*S*,7'*S*,10'*S*,11'*R*).

Artemzhongdianolide B7 (**7**) had a chemical composition of $C_{31}H_{40}O_9$ based on the $[M + HCOO]^-$ ion at *m*/*z* 601.2640 in the (–)-HRESIMS data. The IR absorption bands at 3443, 1765, 1717, 1638, and 947 cm^{-1} indicated the presence of hydroxy, carbonyl, olefinic, and hydroperoxyl groups. The ^{1}H and ^{13}C NMR (DEPT) data of **7** were similar to those of **3**, the main difference was ascribed to the replacement of the carbonyl group at C-3' in **3** by a hydroperoxyl group [δ_H 4.97 (H-3'), δ_C 90.1 (C-3')] in **7**. The correlations of H-6'/H-1''/H-3' in the ROESY spectrum showed that the hydroperoxy group at C-3' was *α*-oriented. The absolute configuration of **7** was assigned though a single crystal X-ray diffraction experiment with Cu Kα radiation [Flack parameter of 0.10(5)], and the absolute configuration of compound **7** was defined as (2*S*,4*S*,6*S*,7*S*,10*S*,1'*R*,3'*R*,6'*S*,7'*S*,10'*S*,11'*R*).

Artemzhongdianolide B8 (**8**) possessed a molecular formula of $C_{31}H_{40}O_9$ according to the HRESIMS data (*m*/*z* 555.2608 $[M–H]^-$). Its IR spectrum showed the characteristic bands of hydroxy (3440 cm^{-1}), carbonyl (1752 cm^{-1}), olefinic (1635 cm^{-1}), and hydroperoxyl (880 cm^{-1}) groups. An analysis of the NMR data of compound **8** suggested a similar structure to compound **7**, with the main differences occurring in the cyclopentane of unit B. Comparison of ^{1}H and ^{13}C NMR (DEPT) spectra between **8** and 7 indicated H_2-2' and OOH-3' in **4** were replaced by a $\Delta^{2'}$ double bond in **8**, which was confirmed by the ^{1}H–^{1}H COSY spin-coupling system of H-2'/H-3' and HMBC cross-peaks H_3-15'/C-3', and H-2'/C-1'/C-10'. In addition, the resonances for a tertiary carbon with a hydroperoxyl group [δ_C 93.8 (C-4')] and a methine [δ_C 52.6 (C-5')] were observed in **8**, instead of signals of a $\Delta^{4'}$ double band in **7**. The CH_2-13'*β* and CH_3-15'*β* configurations were deduced by the ROESY correlations of H_3-15'/H-13'a/H-6'. The correlations of H-7'/H-1''/H_3-14' in the ROESY spectrum showed that CH_3-1'' and CH_3-14' were *α*-oriented. Furthermore, its absolute configuration was also defined as (2*S*,4*S*,6*S*,7*S*,10*S*,1'*S*,4'*S*,5'*R*,6'*S*,7'*S*,10'*S*,11'*R*) by the calculated ECD data.

Artemzhongdianolide B9 (**9**) was obtained as a monoclinic crystal. The molecular formula was designated as $C_{30}H_{34}O_7$ on the basis of protonated ion peak at *m*/*z* 507.2365 $[M + H]^+$, (calcd. 507.2377) in its HRESIMS, suggesting 14 indices of hydrogen deficiency. Comparison of ^{1}H and ^{13}C NMR (DEPT) spectra between **9** and lavandiolide H,[5] indicated that a methylene at C-3 in lavandinolide H was replaced by a carbonyl carbon. Its structure was consolidated by the single-crystal X-ray diffraction analysis [Flack parameter of 0.06(12)] to be (2*S*,4*S*,6*S*,7*S*,10*S*,1'*R*,5'*R*,6'*S*,7'*S*,10'*S*,11'*R*).

Artemzhongdianolide B10 (**10**) gave a molecular formula of

Table 3 ^{1}H NMR data (600 MHz) for compounds **13**—**17** (*J* in Hz)

No.	**13**[b]	**14**[b]	**15**[a]	**16**[b]	**17**[b]
2	2.42 dd (7.8, 1.2)	2.49 dd (8.4, 1.8)	2.33 [c]	2.33 d (9.6)	2.25 d (9.0)
	1.48[c]	1.88 m	1.68 [c]	1.72 dt (2.4, 9.6)	1.63[c]
3	2.59 br s	2.62 br s	2.65 br s	2.70 br d (2.4)	2.62 br s
6	4.98 d (10.8)	5.16 d (10.8)	4.36 d (10.2)	4.34 d (10.2)	4.71 d (10.2)
7	2.71 m	2.88 m	2.74[c]	2.70[c]	2.71 m
8	2.19 m	2.27 m	2.24 m	2.15 m	2.15 m
	1.54 m	1.58 m	1.57 m	1.50 m	1.58 m
9	1.89 m	2.07 m	1.95 m	1.90 m	1.91 m
	1.86 m	1.89 m	1.82 m	1.78 dd (5.4, 14.4)	1.67 m
13	6.27 d (3.0)	6.13 d (3.0)	6.24 d (3.0)	6.22 d (3.0)	6.04 d (3.3)
	5.56 d (3.0)	5.66 d (3.0)	5.55 d (3.0)	5.52 d (3.0)	5.56 d (3.3)
14	1.29 s	1.32 s	1.52 s	1.36 s	1.52 s
15	2.01 d (2.4)	2.02 d (1.8)	1.96 s	1.99 s	1.95 s
2'	2.74[c]	2.56 d (18.0)		2.96 br s	5.93 t (2.4)
	1.48 m	2.30 d (18.0)			
3'	5.55[c]		6.18 s		3.99 d (2.4)
5'	2.80 d (10.2)		3.38 d (9.6)		2.98 d (11.4)
6'	3.90 dd (10.2, 10.2)	5.20 d (10.8)	3.61 dd (10.2, 10.2)	5.15 d (11.4)	4.29 dd (10.5, 10.5)
7'	1.68 m	2.35 td (10.8, 5.4)	2.72 m	2.84 m	2.68 m
8'	1.39 m	1.88 m	1.86 m	1.86 m	1.60 m
	1.22 m	1.50 m	1.16 m	1.83 m	1.57 m
9'	2.05 m	1.96 m	2.35 m	2.51 m	1.84 m
	1.83 m	1.55 m	2.28 m	2.15 m	1.73 m
13'	2.13[c]	2.20 d (12.0)	1.87[c]	2.02[c]	1.98 dd (12.6, 3.0)
	1.61 dd (12.0, 3.0)	1.60 m	1.73 m	1.90[c]	1.72 m
14'	1.27 s	1.19 s	2.38 s	1.84 s	1.38 s
15'	1.94 s	1.77 s	2.31 s	2.04 s	1.32 s

[a] Data were recorded in acetone-d_6. [b] Data were recorded in $CDCl_3$. [c] "ol" is used to indicate overlapped signals, for which the coupling constants could not be read.

$C_{30}H_{34}O_9$ from the (+)-HRESIMS ion at *m/z* 539.2272 ($[M + H]^+$, calcd. 539.2276). By comparing with compound **5**, a methylene at C-3 in **5** was replaced by a carbonyl carbon at C-3 (δ_C 205.6) in **10**. The absolute configuration of compound **10** was elucidated as (2*S*,4*S*,6*S*,7*S*,10*S*,1'*R*,6'*S*,7'*S*,10'*S*,11'*R*) *via* the single-crystal X-ray diffraction experiment [Flack parameter of 0.20(9)] (Figure 4).

Artemzhongdianolide B12 (**12**) had the same molecular formula with **11**. The absorptions at 3435, 1776, and 1649 cm^{-1} in the IR spectrum indicated the presence of hydroxy, carbonyl, and olefinic groups. An analysis of the NMR data of **12** suggested a similar structure to **11**, with the main differences occurring in the cyclopentane ring of unit B. It was observed that a 3',4'-epoxy ring in **11** was replaced by a $\Delta^{3'}$ double bond [δ_H 5.75 (1H, br s, H-3'), δ_C 130.5 (C-3'), 147.6 (C-4')] in **12**. Furthermore, a hydroxy group substituent at C-2' [δ_H 4.14 (1H, d, *J* = 4.8 Hz, H-2'), δ_C 80.3 (C-2')] in **12** was verified by the ^{1}H–^{1}H COSY spin-coupling system of H-2'/H-3' and HMBC cross-peaks H-5'/C-3', and H-3'/C-4'/C-10'. The ROESY correlations of H-7/H_3-14, H-7'/H_3-15, H-5'/H-7'/OH-2', and OH-2'/H_3-14' assigned the α-orientation of CH_3-14/CH_3-15/H-7'/H-5'/CH_3-14'/OH-2', while the cross peak of H-6/H-8/H-11, and H-6'/H-13'a indicated the β-orientation of H-8, H-11, and CH_2-13'. Its absolute configuration was determined as (2*S*,4*S*,6*S*,7*R*,8*S*,10*S*,11*S*,1'*S*,2'*S*,5'*R*,6'*S*,7'*S*,10'*S*,11'*R*) by comparing the experimental ECD spectrum with the calculated one (Figure 5). Artemzhongdianolide B13 (**13**) was obtained as an orthorhombic crystal. The molecular formula was designated as $C_{30}H_{36}O_6$ on the basis of protonated ion peak at *m/z* 493.2566 ($[M + H]^+$, calcd. 493.2585) in its HRESIMS, indicating 13 indices of hydrogen deficiency. The same planar structure of compound **13** with lavandinolide B was determined by detailed interpretation of its 1D and 2D NMR data.[5] Compared with lavandiolide B, the chemical shift of C-13' in **13** was changed to δ_C 32.7 (*vs.* 36.2 in lavandiolide B) revealing the varied stereochemistry. Its structure was consoledated by the single-crystal X-ray diffraction analysis [Flack parameter of 0.073(6)] to be (1*S*,3*R*,6*S*,7*S*,10*R*,1'*R*,5'*R*,6'*S*,7'*S*,10'*S*,11'*S*).

An analysis of the NMR data of artemzhongdianolide B14 (**14**) proposed a similar structure to **13**. The downfield-shifted resonances at C-1' ($\Delta\delta_C$ +4.6) and C-10' ($\Delta\delta_C$ +11.4) suggested the existence of hydroxy group at C-1' and C-10' in **14**. Moreover, it was observed that a $\Delta^{3'}$ double bond in **13** was replaced by a $\Delta^{4'}$ double bond [δ_C 136.6 (C-4'), 167.4 (C-5')], and a carbonyl group at C-3' [δ_C 205.6 (C-3')] in **14**. The absolute configuration of **14** was identified from the similarity between the experimental and calculated ECD spectra.

Artemzhongdianolide B15 (**15**) was obtained as white powders with a molecular formula of $C_{30}H_{34}O_6$ as deduced by the (–)-HRESIMS ion at *m/z* 535.2344 $[M + HCOO]^-$ (calcd. 535.2337), revealing 14 hydrogen deficiency indices. An analysis of the NMR data of **15** suggested it was a sesquiterpenoid dimer. Interpretation of the 2D NMR data of compound **15** indicated that units A and B were deduced as guaianolide moieties. Moreover, ^{1}H–^{1}H COSY correlations of H_2-2/H-3/H_2-13′ combined with the HMBC correlations of H_2-13′/C-1, C-2, and C-4, and of H-3/C-11′ and C-13′ indicated that units A and B were connected *via* two C—C single bonds between C-3—C-13′ and C-1—C-11′, with the six-membered ring formed through a [4+2] cycloaddition reaction.

The relative configuration of compound **15** was partially established by analysis of the ROESY data. The ROESY correlations of H-7/H-2a and H-7′/H-13′a indicated that H-7, CH_2-2, H-7′ and CH_2-13′ were α-orientated, and the ROESY correlations of H-6/H_3-14 assigned H-6 and H_3-14 to be β-orientated. The absolute configuration of compound **15** was determined to be (1*S*,4*R*,6*S*,7*S*,10*R*,5′*S*,6′*S*,7′*S*,11′*S*) by comparison of its experimental ECD spectrum with the calculated one (Figure 5).

Artemzhongdianolide B16 (**16**), a white powder, afforded a molecular formula of $C_{30}H_{34}O_6$ based on the (+)-HRESIMS ion peak at *m/z* 491.2435 $[M + H]^+$ (calcd. 491.2428), corresponding to 14 degrees of hydrogen deficiency. The characteristic IR absorptions demonstrated the presence of hydroxy (3438 cm^{-1}), ester carbonyl (1772, and 1716 cm^{-1}), and olefinic (1634 cm^{-1}) groups. Its ^{1}H and ^{13}C NMR (DEPT) data (Table 3 and 5) were similar to those of compound **15**. It was observed that a $\Delta^{3'}$ double bond in **15** was changed by $\Delta^{4'}$ double bond [δ_C 139.3 (C-4'), δ_C 159.7 (C-5')] in **16** and a carbonyl carbon at C-2' in **15** was replaced by a methylene in **16**. Furthermore, a carbonyl carbon substituted at C-3' in **16**. The ROESY correlations of H-7/H-2a and H-2a/H-13'a assigned the α-orientation of H-7, CH_2-2 and CH_2-13', while the cross peak of H-6/H_3-14 indicated the β-orientation of CH_3-14. Accordingly, the stereochemistry of compound **16** was assigned as (1*S*,4*R*,6*S*,7*S*,10*R*,6′*S*,7′*S*,11′*S*) by comparing the experimental ECD spectrum with the calculated one (Figure 5).

Artemzhongdianolide B17 (**17**) possessed a molecular formula of $C_{30}H_{38}O_8$ according to the HRESIMS data (*m/z* 571.2561 $[M + HCOO]^-$). Its IR spectrum showed the characteristic bands of

Table 4 ^{13}C NMR data (150 MHz) for compounds **1**—**9** (δ)

No.	1[a]	2[a]	3[b]	4[b]	5[b]	6[b]	7[b]	8[b]	9[b]
1	71.4, C	71.4, C	151.9, C	150.3, C	151.9, C	150.8, C	151.6, C	150.0, C	144.8, C
2	39.3, CH_2	39.3, CH_2	43.0, CH	42.6, CH	43.0, CH	42.5, CH	43.0, CH	43.3, CH	47.3, CH
3	126.3, CH	126.3, CH	53.2, CH_2	54.0, CH_2	53.3, CH_2	53.5, CH_2	53.3, CH_2	53.6, CH_2	201.5, C
4	141.3, C	141.2, C	60.5, C	61.4, C	60.4, C	60.5, C	60.3, C	63.0, C	57.5, C
5	52.4, CH	52.5, CH	144.2, C	145.0, C	144.1, C	144.3, C	144.4, C	145.0, C	139.4, C
6	83.3, CH	83.3, CH	83.5, CH	84.5, CH	83.5, CH	84.5, CH	83.8, CH	84.3, CH	81.5, CH
7	165.2, C	164.9, C	46.8, CH	47.7, CH	46.8, CH	47.7, CH	46.9, CH	47.3, CH	46.4, CH
8	22.7, CH_2	22.7, CH_2	23.5, CH_2	24.6, CH_2	23.6, CH_2	24.5, CH_2	23.6, CH_2	24.4, CH_2	23.5, CH_2
9	31.3, CH_2	31.4, CH_2	38.6, CH_2	39.8, CH_2	38.5, CH_2	40.0, CH_2	38.6, CH_2	38.8, CH_2	38.6, CH_2
10	62.1, C	62.1, C	72.8, C	73.6, C	72.8, C	73.5, C	72.7, C	72.3, C	73.6, C
11	126.5, C	126.7, C	140.1, C	139.8, C	140.3, C	139.8, C	140.2, C	139.8, C	139.5, C
12	173.9, C	173.9, C	170.2, C	170.4, C	170.3, C	170.4, C	170.4, C	170.4, C	169.4, C
13	18.3, CH_2	17.6, CH_2	119.2, CH_2	119.1, CH_2	119.3, CH_2	119.1, CH_2	119.1, CH_2	119.3, CH_2	120.0, CH_2
14	22.4, CH_3	22.4, CH_3	27.3, CH_3	27.6, CH_3	27.4, CH_3	27.6, CH_3	27.4, CH_3	28.8, CH_3	27.0, CH_3
15	18.6, CH_3	18.6, CH_3	17.4, CH_3	17.9, CH_3	17.4, CH_3	17.4, CH_3	17.4, CH_3	18.1, CH_3	10.8, CH_3
1'	72.8, C	72.8, C	84.9, C	88.4, C	80.2, C	80.3, C	91.0, C	93.9, C	72.4, C
2'	40.2, CH_2	40.1, CH_2	41.4, CH_2	41.8, CH_2	46.7, CH_2	46.7, CH_2	35.8, CH_2	133.7, CH	39.5, CH_2
3'	125.7, CH	125.9, CH	204.4, C	205.3, C	205.6, C	205.2, C	90.1, CH	141.4, CH	125.4, CH
4'	141.5, C	141.3, C	141.2, C	147.4, C	138.1, C	138.4, C	141.3, C	93.8, C	140.5, C
5'	52.8, CH	53.4, CH	162.4, C	159.0, C	165.6, C	165.5, C	136.5, C	52.6, CH	51.5, CH
6'	82.2, CH	80.3, CH	75.6, CH	78.9, CH	76.0, CH	75.7, CH	75.8, CH	81.7, CH	80.8, CH
7'	53.8, CH	58.4, CH	50.3, CH	42.8, CH	50.4, CH	50.3, CH	51.1, CH	42.0, CH	52.8, CH
8'	18.8, CH_2	19.3, CH_2	20.9, CH_2	22.6, CH_2	21.0, CH_2	21.1, CH_2	21.2, CH_2	26.2, CH_2	18.5, CH_2
9'	33.8, CH_2	33.8, CH_2	34.2, CH_2	38.2, CH_2	34.5, CH_2	34.4, CH_2	33.9, CH_2	35.6, CH_2	32.9, CH_2
10'	63.0, C	62.9, C	73.6, C	76.2, C	73.4, C	73.5, C	74.8, C	76.8, C	62.4, C
11'	76.2, C	76.6, C	57.0, C	56.3, C	57.0, C	56.8, C	57.0, C	55.5, C	51.5, C
12'	177.0, C	177.5, C	180.2, C	179.7, C	180.3, C	179.1, C	181.1, C	182.2, C	178.6, C
13'	33.6, CH_2	30.7, CH_2	35.0, CH_2	34.2, CH_2	34.8, CH_2	34.6, CH_2	34.8, CH_2	35.9, CH_2	30.8, CH_2
14'	22.9, CH_3	22.8, CH_3	27.4, CH_3	29.0, CH_3	27.2, CH_3	27.2, CH_3	27.4, CH_3	30.0, CH_3	22.7, CH_3
15'	18.6, CH_3	18.5, CH_3	8.7, CH_3	9.6, CH_3	8.8, CH_3	8.9, CH_3	12.1, CH_3	19.0, CH_3	18.4, CH_3
1''			51.0, OCH_3	50.9, OCH_3			50.7, OCH_3	51.0, OCH_3	

[a] Data were recorded in acetone-d_6. [b] Data were recorded in $CDCl_3$.

Scheme 1 Hypothetical biosynthetic pathways for compounds **1** and **2**

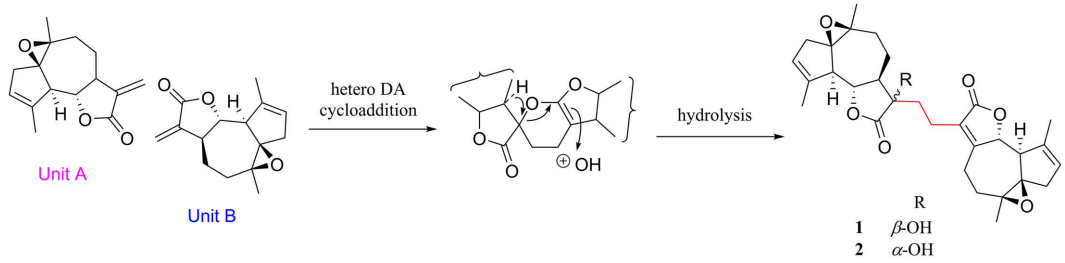

hydroxy (3434 cm^{-1}), carbonyl (1767, and 1736 cm^{-1}), and olefinic (1631 cm^{-1}) groups. An analysis of the NMR data of compound **17** suggested a similar structure to compound **15**, with the main differences occurring in the cyclopentane of unit B. Comparison of ^1H and ^{13}C NMR (DEPT) spectra between **17** and **15** indicated $\Delta^{3'}$ double bond in **15** was replaced by OH-3' [δ_H 3.99 (1H, d, J = 2.4 Hz, H-3'), δ_C 80.3 (C-3')] and OH-4' [δ_C 80.8 (C-4')] in **17**, and carbonyl carbon at C-2' and $\Delta^{1'10'}$ double bond in **15** were replaced by $\Delta^{1'}$ double bond [δ_H 5.93 (1H, t, J = 2.4 Hz, H-2'), δ_C 152.6 (C-1'), δ_C 127.9 (C-2')] and OH-10' [δ_C 70.8 (C-10')], which was confirmed by the ^1H–^1H COSY spin-coupling system of H-2'/H-3' and HMBC cross-peaks H_3-15'/C-4'/C-3', H_3-14'/C-1'/C-10', and H-6'/C-1'/C-4'. Its relative configurations were defined by the ROESY correlations of H-6/H_3-14, H-6'/H-3'/H_3-15'/H-13'a, H-7/H-2a, H-7'/H-13'a and H-5'/H_3-14'. Furthermore, its absolute configuration was also defined as (1*S*,4*R*,6*S*,7*S*,10*R*,3'*R*,4'*S*,5'*S*,6'*S*,7'*S*,10'*S*,11'*S*) by the calculated ECD data.

Compounds **1**—**2** represent a new type of dimeric sesquiterpenoid. A putative biosynthetic route of them was proposed as shown in Scheme 1, in which compounds **1** and **2** were presumebly derived from arglabin. The hetero DA cycloaddition between two arglabin generated compounds **1** and **2** with the formation of a C—C bond.

The EtOH extract and EtOAc fraction showed cytotoxicity against HepG2 cells with inhibitory ratios of 81.6% and 75.4% at 200.0 μg/mL. After separation, Frs. A—G were assayed for the antihepatoma activity to suggest that the fractions A—E showed better inhibitory ratios of 60.9, 68.6, 75.9, 81.7 and 83.7 at 100.0 μg/mL in HepG2 cells, respectively.

The cytotoxicity of all isolated GSDs (**1**—**17**) against three

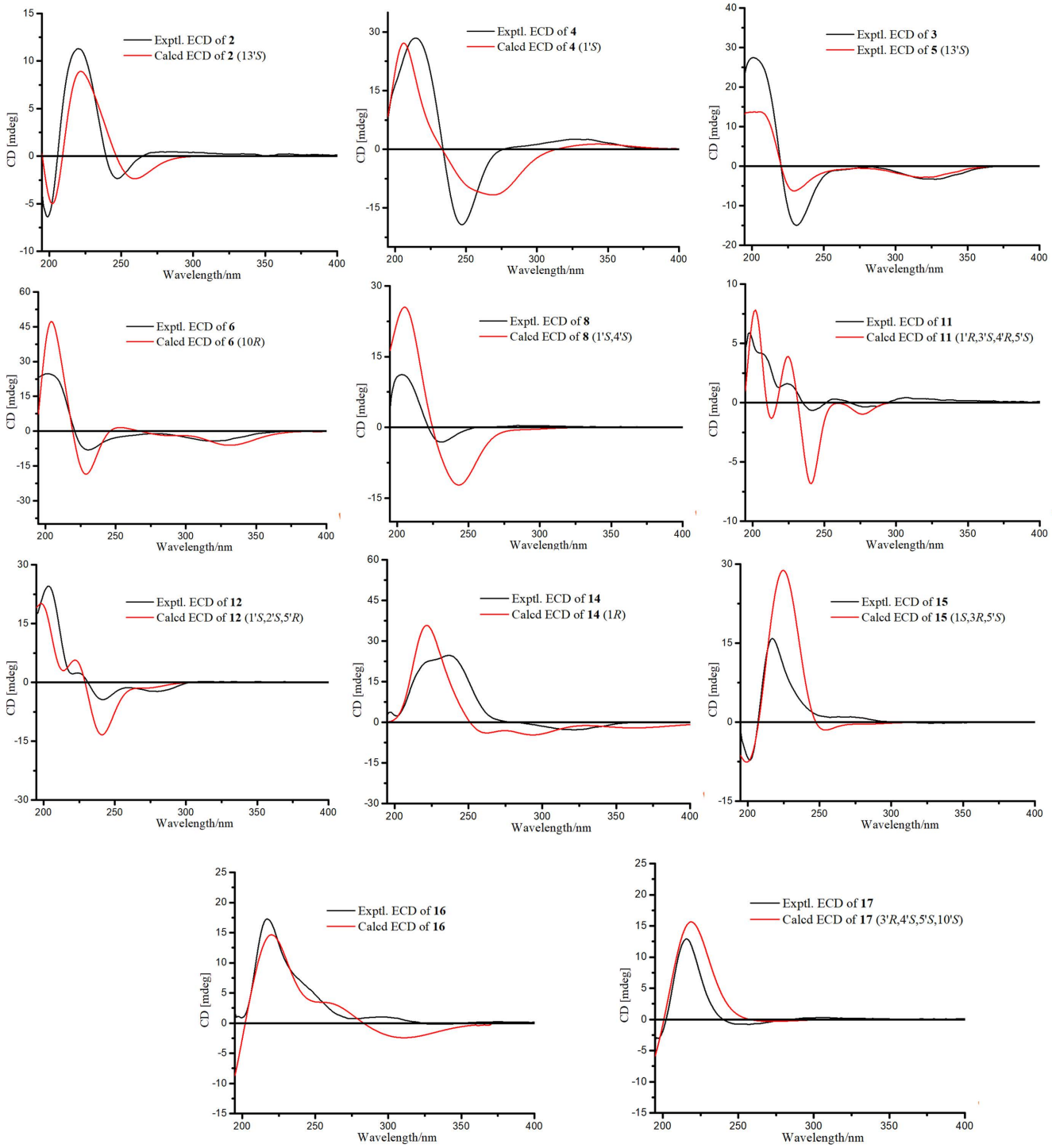

Figure 5 The experimental and calculated ECD spectra of compounds **2**, **4**—**6**, **8**, **11**, **12** and **14**—**17**.

hepatoma cell lines (HepG2, Huh7, and SK-Hep-1) was evaluated, and the results are shown in Table 6. Most of them exhibited significant cytotoxic effects. Compounds **3** and **9** showed cytotoxicity on HepG2 cells, with IC_{50} values of 9.9 and 13.1 μmol/L, respectively, which are comparable to that of sorafenib (IC_{50} = 11.9 μmol/L); compounds **4**, **5**, **7** and **13** exhibited moderate cytotoxicity with IC_{50} values in the range of 21.1 to 40.3 μmol/L. Compounds **6**, **8**, and **15** displayed cytotoxicity with IC_{50} values of 50.2, 54.7, and 140.3 μmol/L, respectively.

Compounds **3**, **9**, and **15** exhibited comparable cytotoxicity to sorafenib, with IC_{50} values of 18.6, 19.5, and 18.7 μmol/L in Huh7 cells, respectively; Compounds **4**—**7** displayed moderate cytotoxicity with IC_{50} values ranging from 30.9 to 47.2 μmol/L, and compounds **8** and **13** showed cytotoxicity with IC_{50} values of 77.5 and 59.1 μmol/L, respectively.

For SK-Hep-1 cells, compounds **9** and **13** displayed significant activity with IC_{50} values of 19.5 and 17.9 *μ*mol/L, respectively, comparable to that of sorafenib (IC_{50}, 12.2 μmol/L); Compounds **3** and **15** showed moderate cytotoxicity with IC_{50} values of 35.1 to 37.6 μmol/L, and compounds **4**—**8** possessed activity with IC_{50} values ranging from 50.3 to 170.1 μmol/L.

This series of compounds could help us to figure out the structure-activity relationships. Firstly, compound **3** (IC_{50}, 9.9 μmol/L in HepG2, 18.6 μmol/L in Huh7 and 35.1 μmol/L in SK-Hep-1) with a *β*-OMe group at C-1' possessed 1.5 to 4 times stronger activity than compound **4** (IC_{50}, 40.3 μmol/L in HepG2, 44.3 μmol/L in Huh7 and 89.4 μmol/L in SK-Hep-1), which suggested that the *β*-OMe instead of *α*-OMe was favorable for

Table 5 ^{13}C NMR data (150 MHz) for compounds **10**—**17** (δ)

No.	**10**[a]	**11**[b]	**12**[a]	**13**[b]	**14**[a]	**15**[b]	**16**[b]	**17**[a]
1	148.1, C	143.7, C	146.2, C	65.5, C	66.6, C	71.6, C	71.2, C	72.5, C
2	47.9, CH	46.9, CH	47.8, CH	46.8, CH_2	48.0, CH_2	47.7, CH_2	47.6, CH_2	48.0, CH_2
3	201.5, C	201.2, C	201.9, C	57.9, CH	58.0, CH	45.4, CH	45.6, CH	46.1, CH
4	57.8, C	57.6, C	57.8, C	141.0, C	141.4, C	143.4, C	142.2, C	142.2, C
5	138.6, C	139.9, C	139.7, C	135.2, C	136.9, C	134.7, C	134.7, C	136.6, C
6	81.9, CH	78.2, CH	79.1, CH	84.0, CH	84.4, CH	82.8, CH	82.4, CH	83.0, CH
7	47.0, CH	56.2, CH	57.2, CH	45.1, CH	46.0, CH	51.4, CH	51.6, CH	52.2, CH
8	24.0, CH_2	71.8, CH	71.8, CH	25.1, CH_2	25.8, CH_2	24.1, CH_2	24.0, CH_2	24.4, CH_2
9	31.7, CH_2	49.8, CH_2	50.2, CH_2	39.3, CH_2	40.7, CH_2	41.2, CH_2	41.0, CH_2	42.1, CH_2
10	73.4, C	71.8, C	72.0, C	72.7, C	72.6, C	74.0, C	73.9, C	74.6, C
11	141.4, C	41.9, CH	42.3, CH	138.2, C	140.2, C	138.8, C	138.8, C	140.8, C
12	169.5, C	178.1, C	178.6, C	169.7, C	169.7, C	169.7, C	169.9, C	169.8, C
13	119.2, CH_2	15.5, CH_3	15.7, CH_3	120.8, CH_2	120.0, CH_2	120.5, CH_2	120.3, CH_2	118.9, CH_2
14	26.8, CH_3	29.1, CH_3	29.0, CH_3	26.7, CH_3	26.4, CH_3	28.8, CH_3	28.6, CH_3	29.0, CH_3
15	11.1, CH_3	10.9, CH_3	11.2, CH_3	17.4, CH_3	17.4, CH_3	14.4, CH_3	14.6, CH_3	14.4, CH_3
1'	80.7, C	69.3, C	74.3, C	72.9, C	77.5, C	131.4, C	128.6, C	152.6, C
2'	47.2, CH_2	36.3, CH_2	80.3, CH	39.5, CH_2	47.3, CH_2	195.7, C	40.3, CH_2	127.9, CH
3'	205.6, C	62.7, CH	130.5, CH	125.0, CH	205.6, C	136.3, CH	204.4, C	80.3, CH
4'	137.0, C	65.7, C	147.6, C	141.7, C	136.6, C	169.4, C	139.3, C	80.8, C
5'	166.1, C	50.3, CH	51.1, CH	53.3, CH	167.4, C	53.4, CH	159.7, C	60.1, CH
6'	77.2, CH	78.6, CH	81.2, CH	81.5, CH	77.5, CH	84.4, CH	80.8, CH	82.4, CH
7'	50.0, CH	51.1, CH	51.8, CH	53.8, CH	52.1, CH	55.6, CH	45.9, CH	52.2, CH
8'	19.0, CH_2	18.2, CH_2	19.1, CH_2	21.4, CH_2	21.7, CH_2	24.1, CH_2	24.6, CH_2	22.0, CH_2
9'	34.6, CH_2	32.7, CH_2	33.8, CH_2	34.1, CH_2	35.1, CH_2	37.5, CH_2	33.8, CH_2	40.3, CH_2
10'	73.9, C	59.2, C	64.4, C	62.6, C	74.0, C	153.1, C	134.6, C	70.8, C
11'	53.1, C	51.5, C	52.1, C	52.5, C	54.7, C	57.0, C	56.2, C	57.2, C
12'	177.8, C	178.3, C	178.0, C	181.9, C	181.6, C	184.5, C	184.4, C	186.6, C
13'	39.1, CH_2	30.8, CH_2	31.1, CH_2	32.7, CH_2	33.1, CH_2	35.2, CH_2	35.4, CH_2	36.0, CH_2
14'	26.5, CH_3	22.7, CH_3	23.2, CH_3	22.5, CH_3	26.3, CH_3	21.4, CH_3	24.5, CH_3	30.7, CH_3
15'	8.6, CH_3	18.8, CH_3	18.8, CH_3	18.7, CH_3	8.5, CH_3	22.3, CH_3	9.9, CH_3	22.0, CH_3

[a] Data were recorded in acetone-d_6. [b] Data were recorded in $CDCl_3$.

Table 6 Cytotoxicity of compounds from *A. zhongdianensis*

Compound	IC_{50}[a]/(μmol·L^{-1})		
	HepG2	Huh7	SK-Hep-1
3	9.9 ± 2.0	18.6 ± 2.9	35.1 ± 2.7
4	40.3 ± 2.1	44.3 ± 1.6	89.4 ± 2.2
5	29.3 ± 1.9	38.8 ± 1.9	50.3 ± 2.4
6	50.2 ± 3.2	47.2 ± 2.1	58.4 ± 2.0
7	21.1 ± 2.0	30.9 ± 2.7	58.4 ± 1.7
8	54.7 ± 2.6	77.5 ± 1.9	170.1 ± 3.2
9	13.1 ± 1.5	19.5 ± 2.8	19.5 ± 1.8
13	22.1 ± 1.5	59.1 ± 1.6	17.9 ± 1.4
15	140.3 ± 5.5	18.7 ± 4.2	37.6 ± 1.8
Sorafenib[b]	11.9 ± 2.3	12.2 ± 2.3	12.2 ± 2.0

[a] Data were expressed as means ± SD (n = 3). [b] Sorafenib was used as a positive control.

increasing activity. Secondly, compound **5** (IC_{50}, 29.3 μmol/L in HepG2, 38.8 μmol/L in Huh7 and 50.3 μmol/L in SK-Hep-1) with a α-Me group at C-10 exhibited higher cytotoxicity than compound **6** (IC_{50}, 50.2 μmol/L in HepG2, 47.2 μmol/L in Huh7 and 58.4 μmol/L in SK-Hep-1), which suggested that the β-Me was favorable. Thirdly, compound **3** (IC_{50}, 9.9 μmol/L in HepG2, 18.6 μmol/L in Huh7 and 35.1 μmol/L in SK-Hep-1) with a methoxy group at C-1' was approximately 1.5 to 3 times potent than compound **5** (IC_{50}, 29.3 μmol/L in HepG2, 38.8 μmol/L in Huh7 and 50.3 μmol/L in SK-Hep-1) with a hydroxy group at C-1', which indicated that hydroxy group was unfavorable.

These results indicated that compound **9** showed the highest cytotoxicity against HepG2, Huh7, and SK-Hep-1 cells with IC_{50} values of 13.1, 19.5, and 19.5 μmol/L, respectively. Herein, there was a major interest to explore the pharmacological mechanism of compound **9** in inhibition of HCC.

To further elucidate the target proteins and pathway of the compound **9**, machine learning approach was adopted to predict the targets of **9**. The known 11 416 drug-target interactions among 2 228 drugs and 2 869 proteins were collected from DrugBank as the training positive data in January, 2022. The randomly selected drug-protein pairs were selected as the training negative data. The compound chemical structure and protein amino acid sequence were introduced to represent compound and protein, respectively. The random forest algprithm was used to predict the protein targets of compound **9**. The potential target proteins were selected form the top five predict ions that were closely associated with cancer. According to the Uniprot database, the predicted third-ranked target gene P46734 was associated with tumors (Figure 6 A). The P46734 coding gene is mitogen-activated protein kinase kinase 3 (*MAP2K3*, also known as *MKK3*). *MAP2K*3 displayed significantly different expression level between liver cancer tumors and normal controls (Figure 6 B) base on the TCGA liver cancer data portal. Mice lacking *MAP2K3* and *MKK6* showed a higher tendency for tumor proliferation.[24] *MAP2K3* catalyzes the concomitant phosphorylation of a threonine and a tyrosine

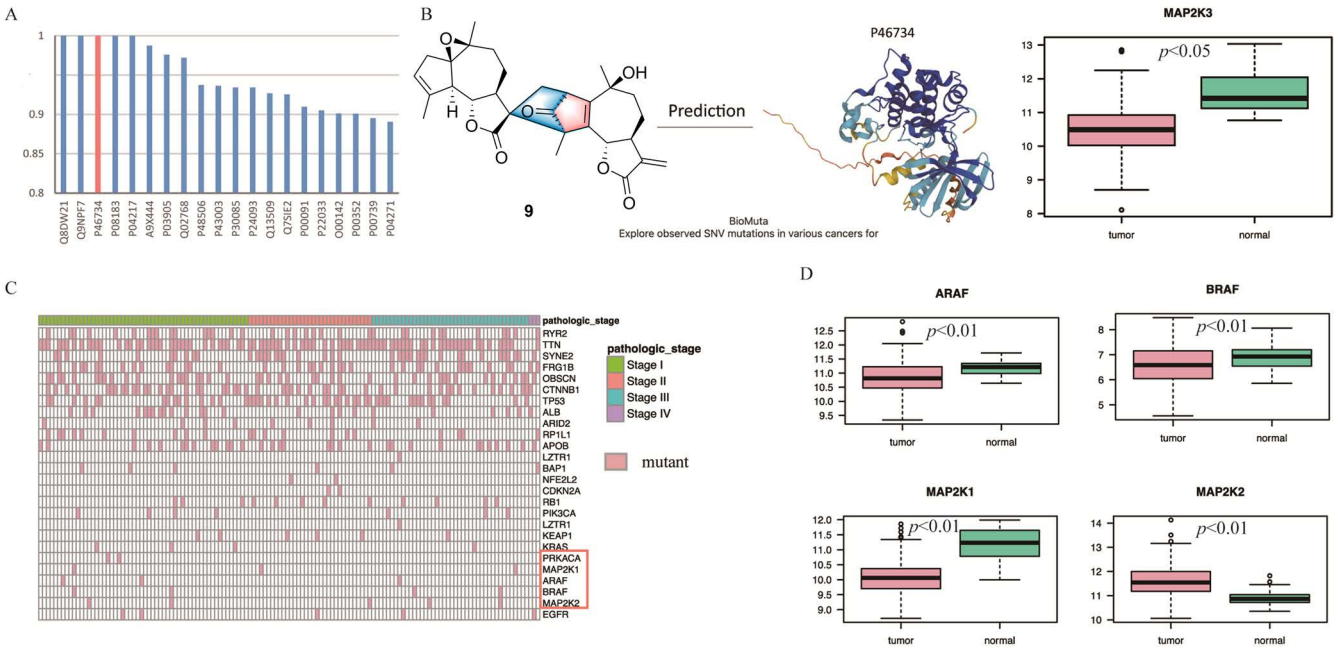

Figure 6 The predicted target protein for compound **9**. A, The top 20 predicted targets for compound **9**. The closer to 1 prediction score means the higher probability of the targets interaction with compound **9**. B, the chemical structure for compound **9** and protein structure for its predicted target P46734. The expression level for P46734 coding gene *MAP2K3* in liver cancer tumors and adjacent normal tissues. The molecular characteristics for TCGA liver cancer patients. C, the heatmap shows the mutation profile for top mutant genes in TCGA liver cancer patients. Genes involved in MAPK signaling pathway were highlighted by red square. The tumor stage was also indicated *via* different color. D, the expression level for genes involved in MAPK signaling pathway in liver cancer tumors and adjacent normal tissues.

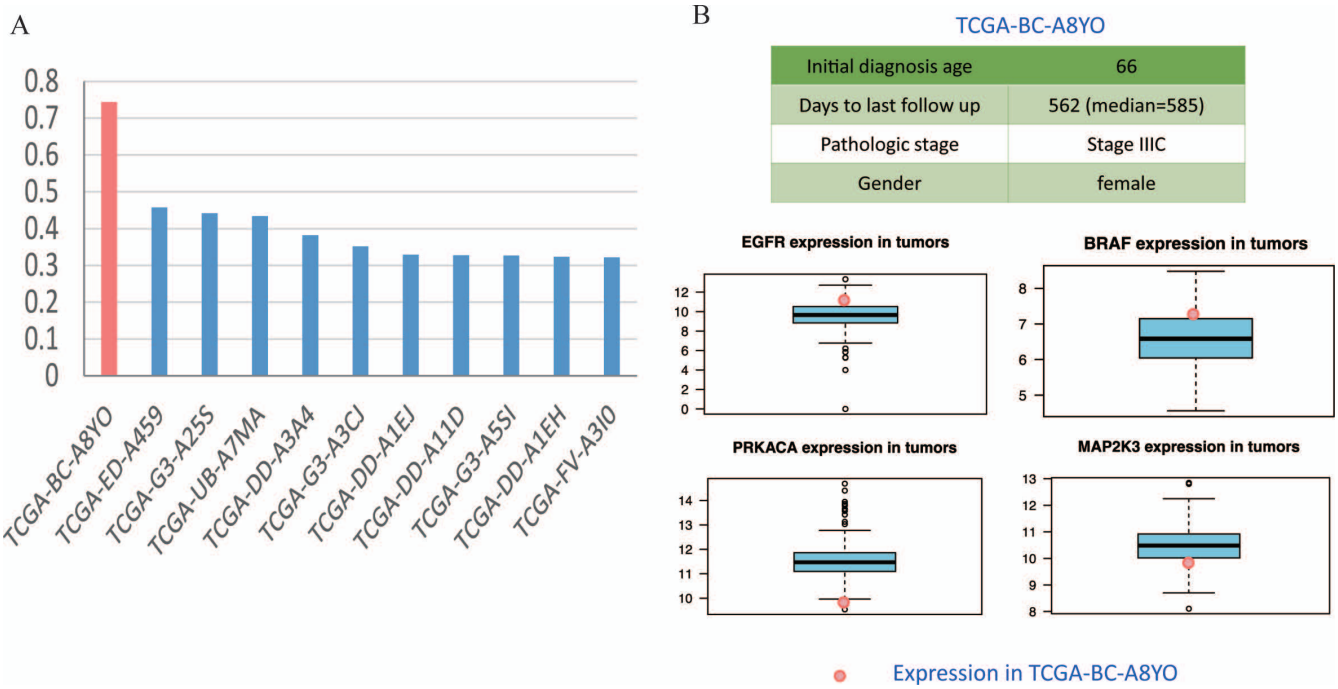

Figure 7 The predicted liver cancer patients that will be sensitive to compound **9** of treatment. A, the prediction score for HCC patients, which may be sensitive to the treatment of compound **9**. HCC tumor patients with a predictive value closer to 1 are more likely to be effective with compound **9** interventions. B, the clinical and molecular properties for patients that have good response to compound **9** of treatment. The patient with poor survival, high tumor grade, and relative high expression level in oncogene EGFR and BRAF, low expression level in MAPK signaling pathway genes has high probability to sensitize compound **9** of treatment.

residue in the p38MAPK. The role of p38 as an antitumorigenic factor had been extensively studied. Some experiments using mouse models of cancer showed that p38MAPK suppresses liver tumor formation *in vivo*.[25] Furthermore, there were three other genes, *ARAF*, *BRAF*, *MAP2K1* in MAPK signaling pathway, differentially expressed in liver cancer tumors, which were also mutant in liver tumors (Figures 6C—D). Moreover, the prediction results showed that the patient with poor survival, high tumor grade, and relative high expression level in oncogene EGFR and BRAF, low expression level in MAPK signaling pathway genes had high probability to sensitize compound **9** treatment (Figures 7 A—B).

In total, p38MAPK pathway might play an important role in

responding to compound **9**. To verify the above bioinformatics analysis results, a series of experiments of artemzhongdianolide B9 (**9**) in HepG2 cells were carried out. Firstly, cell migration and invasion are critical components in cancer metastasis. Transwell assays were performed to assess the impact of compound **9** on HCC metastasis. The migration ratio was decreased to 58.7%, 37.8% and 17.9% at 6.0, 12.0 and 18.0 μmol/L, respectively, indicating a reduction compared to control group. The invasion cell ratio was reduced from 32.9% to 9.8%, 32.9% (6.0 μmol/L), 25.4% (12.0 μmol/L) and 9.8% (18.0 μmol/L). These data showed that compound **9** significantly inhibited HCC cells metastasis *in vitro* (Figures 8A—B).

Because the antiproliferative effect is related to cell cycle and apoptosis, Flow cytometer (FACS) was used to analyze the effects of the cell cycle progression and apoptosis on HepG2 cells. FACS results indicated that the G1 phase cell percentage increased from 46.4% in the control group to 52.6% (6.0 μmol/L), 64.7% (12.0 μmol/L) and 67.5% (18.0 μmol/L) (Figures 8C—D). The results revealed that compound **9** interfered G1 phase transition in HepG2 cells. The Western blot was employed to analyze the effect of compound **9** on cell cycle-key protein, which showed that compound **9** could downregulate the proteins level of CDK4, CDK6 and CyclinD1 and upregulate the expression of P21 in a concentration-dependent manner (Figures 8E—F).

Furthermore, Flow cytometry analysis revealed that apoptotic cells in HepG2 cells increased with the increasing concentration of artemzhongdianolide B9 from 9.0% (6.0 μmol/L) to 31.5% (12.0 μmol/L), and 37.4% (18.0 μmol/L), compared to control cells, as shown in Figures 8G—H. In addition, The Western blot was employed to estimate the levels of Bax and Bcl-2 which were indicators of apoptosis in Figures 8I—J. Artemzhongdianolide B9 promoted the expression level of Bax and inhibited the protein level of Bcl-2 in a dose-dependent manner. In summary, these results demonstrated that compound **9** inhibited the growth of HepG2 cells through arresting the cells at G1 phase and inducing cell apoptosis.

The bioinformatic analysis indicated that artemzhongdianolide B9 (**9**) might inhibit hepatoma by upregulating the p38MAPK signaling pathway. In order to validate that mechanism, the Western blot experiment was implemented. It was found that artemzhongdianolide B9 (**9**) significantly increased the protein expression of p-p38 (Thr180 and Tyr182) in a dose-dependent manner but failed to alter the expression of total p38 with the treatment of compound **9** in HepG2 cells (Figures 8K—L). Taken together, artemzhongdianolide B9 offers a promising agent in the treatment of patients with liver cancer.

Conclusions

As a summary, 17 new GSDs were isolated from the active fractions of *A. zhongdianensis* under the guidance of LC-MS and bioassay, and were structurally elucidated by UV, IR, MS, NMR spectral data, X-ray crystallographic analysis, and ECD calculations. To our best knowledge, artemzhongdianolides B1 (**1**) and B2 (**2**) are the first example of the GSDs fused *via* a C-13/C-13' single bond. Importantly, two compounds (**3** and **9**) showed obvious activities

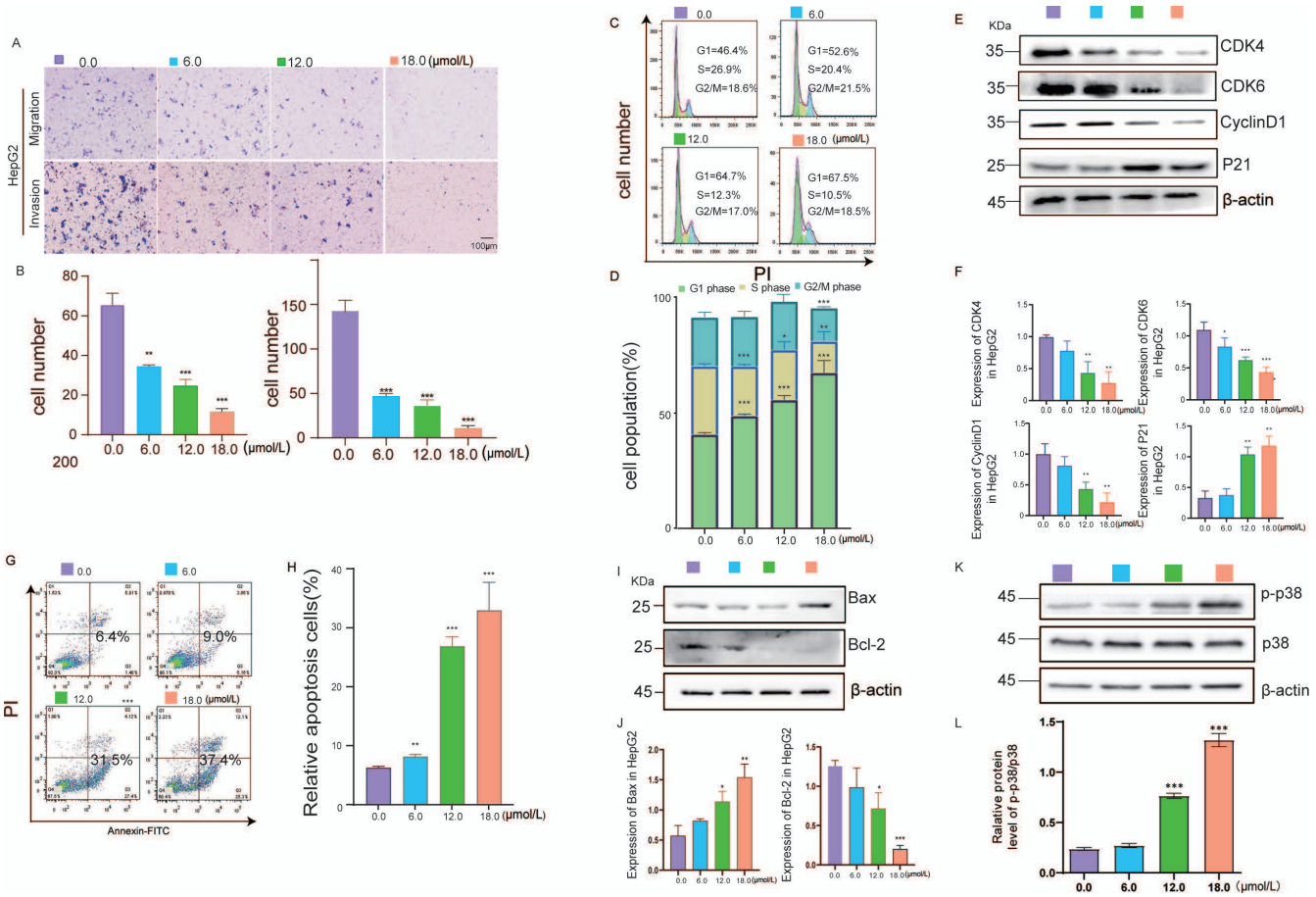

Figure 8 Compound **9** restrained the migration and invasion, cell cycle arrest and apoptosis on HepG2 cells. HepG2 cells were treated with different concentrations (0.0, 6.0, 12.0 and 18.0 μmol/L) of compound **9** for 48 h. (A) Representative photographs of Transwell assay showed migrating and invading cells after incubation. (B) Histogram of migrating and invading cells after incubation. *$p < 0.05$, **$p < 0.01$, and *** $p < 0.001$, $n = 3$. (C) and (D) Flow cytometric analysis and cell cycle quantification of HepG2 cells. (E) and (F) Western blot and statistical results of CDK4, CDK6, CyclinD1 and P21. *$p < 0.05$, **$p < 0.01$, and ***$p < 0.001$, $n = 3$. (G) and (H) Flow cytometric analysis and cell cycle quantification of HepG2 cells. (I) and (J) Western blot and statistical results of CDK4, CDK6, CyclinD1 and P21. *$p < 0.05$, **$p < 0.01$, and ***$p < 0.001$, $n = 3$. K, Western blot was used to measure the proteins of p38 and p-p38 (Thr180/Tyr182). L, the results were represented as the mean ± SD for each group ($n = 3$). *$p < 0.05$; **$p < 0.01$; ***$p < 0.001$ versus control.

against HepG2 cells with IC_{50} values comparable to that of sorafenib, three compounds (**3**, **9**, and **16**) exhibited cytotoxicity against Huh7 cells with IC_{50} values equivalent to that of sorafenib, and two compounds (**9**, and **13**) showed potential effects against SK-Hep-1 cells with IC_{50} values of 19.5, and 17.9 μmol/L. Markedly, artemzhongdianolide B9 was the most active one against three hepatoma cell lines and dose-dependently inhibited cell migration and invasion, induced G1 cell cycle arrest in HepG2 cells by downregulating CDK4, CDK6 and CyclinD1 proteins expression and upregulating the level of P21 protein, and induced cell apoptosis by promoting the expression level of Bax and inhibiting the protein level of Bcl-2 in a dose-dependent manner. Furthermore, machine learning prediction results showed that artemzhongdianolide B9 might inhibit HepG2 cells by regulating the p38MAPK pathway, artemzhongdianolide B9 was exerted antihepatoma effect through significantly activating the p38MAPK pathway. Our research enriched the structural type of sesquiterpenoid dimers in nature and revealed active constituents of *A. zhongdianensis* against hepatoma, and suggested artemzhongdianolide B9 was a promising candidate for liver cancer treatment.

Experimental

General experimental procedures, plant materials, and cytotoxicity, flow cytometer, cell migration and invasion assays were in accordance with the previous reports,[5,15,21] and provided in Supporting Information.

Extraction and isolation

Based on our previous report (see Supporting Information),[21] Frs. A—G were assayed for the antihepatoma activity to suggest that the fractions A—E showed better inhibitory activity than fractions F—G with ratios of 60.9%, 68.6%, 75.9%, 81.7% and 83.7% at 100.0 μg/mL in HepG2 cells. The Fr. C (117 g) was chromatographed on silica gel column (1.0 kg, 9.5 × 60 cm) with a step gradient mixture of EtOAc–PE (5 : 95, 10 : 90 and 20 : 80) to obtain fractions C1—C5 (10, 27, 37, 20 and 16 g). The Fr. C5 (16 g) was submitted to silica gel column (200 g, 5 × 40 cm) with a step gradient mixture of EtOAc–$CHCl_3$ (2 : 98, 10 : 90 and 20 : 80) to afford fractions C5.1—C5.3 (1.5 g, 9.8 g and 4.5 g). The Fr. C5.2 (9.8 g) was separated by MPLC on a RP-C18 column (100 g, 3.0 × 40 cm) and eluted with H_2O–MeOH gradient (70 : 30, 50 : 50, 30 : 70 and 0 : 100) to give fractions C5.2.1—C5.2.4. The Fr. C5.2.4 (1.5 g) was separated into five subfractions (Frs. C5.2.4.1—C5.2.4.5) on Si CC (30 g, 2.5×25 cm) using a gradient of EtOAc–$CHCl_3$ (2 : 98 to 10 : 90). Compounds **3** (5 mg, t_R = 17 min) and **7** (6 mg, t_R = 19 min) were obtained from Fr. C5.2.4.4 (190 mg) by preparative HPLC (H_2O–CH_3CN, 50 : 50, 10.0 mL/min) and semi-preparative HPLC (H_2O–CH_3CN, 60 : 40, 3.0 mL/min). Compounds **4** (2 mg, t_R = 11 min), **5** (3 mg, t_R = 9 min), **6** (8 mg, t_R = 7 min) and **8** (2 mg, t_R = 18 min) were acquired from Fr. C5.2.4.5 (250 mg) by preparative HPLC (H_2O–CH_3CN, 63 : 37, 10.0 mL/min) and semi-preparative HPLC (H_2O–CH_3CN, 57 : 43, 3.0 mL/min). Compound **11** (5 mg, t_R = 11 min) was obtained from Fr. C5.2.2.5 (350 mg) by preparative HPLC (H_2O–CH_3CN, 46 : 54, 10.0 mL/min) and semi-preparative HPLC (H_2O–MeOH, 51 : 49, 3.0 mL/min).

The Fr. D (79 g) was fractionated by MPLC on an MCI gel CHP 20P column (490 g, 5 × 50 cm) eluting with a gradient solvent of H_2O–MeOH (70 : 30, 50 : 50, 30 : 70 and 0 : 100) to provide four subfractions (Fr. D1—Fr. D4). The Fr. D2 (21 g) was chromatographed on silica gel column (200 g, 5 × 40 cm) with a step gradient mixture of acetone–$CHCl_3$ (2 : 98, 10 : 90 and 20 : 80) to obtain fractions D2.1—D2.5 (4.5 g, 3.9 g, 5.5 g, 3.5 g and 3.7 g). The Fr. D2.5 (3.7 g) was separated into five subfractions (Frs. D2.5.1—D2.5.5) on Si CC (40 g, 2.5 × 25 cm) using a gradient of EtOAc–$CHCl_3$ (2 : 98 to 10 : 90). Compounds **10** (13 mg, t_R = 14.0 min), **12** (6 mg, t_R = 16.5 min) and **14** (4 mg, t_R = 20.5 min) were acquired from Fr. D2.5.2 (512 mg) by Sephadex LH-20 CC (140 g, 2.5 × 140 cm, MeOH–$CHCl_3$, 50 : 50) and semi-preparative HPLC (H_2O–MeOH, 46 : 54). The Fr. D3 (19 g) was chromatographed on silica gel column (200 g, 5 × 40 cm) with a step gradient mixture of acetone–$CHCl_3$ (2 : 98, 10 : 90 and 20 : 80) to obtain fractions D3.1—D3.5 (3.3 g, 1.7 g, 2.0 g, 6.4 g and 4.0 g). The Fr. D3.1 (3.3 g) was separated into five subfractions (Fr. D3.1.1—D3.1.5) on Si CC (40 g, 2.5×25 cm) using a gradient of acetone–PE (2 : 98 to 10 : 90). Compounds **1** (17 mg, t_R = 20 min), **2** (11 mg, t_R = 21.2 min), and **13** (12 mg, t_R = 18 min) were obtained from Fr. D3.1.2 (900 mg) by preparative HPLC (H_2O–CH_3CN, 25 : 75, 10.0 mL/min) and semi-preparative HPLC (H_2O–CH_3CN, 37 : 63, 3.0 mL/min). Fraction D3.1.4 (450 mg) was separated by reparative HPLC (H_2O–CH_3CN, 25 : 75, 10.0 mL/min) and semi-preparative HPLC (H_2O–CH_3CN, 51 : 49, 3.0 mL/min) to give compounds **9** (30 mg, t_R = 18 min), **15** (12 mg, t_R = 18 min), **16** (4 mg, t_R = 19.5 min), and **17** (4 mg, t_R = 24 min).

Compound characterization

Artemzhongdianolide B1 (1). Colorless monoclinic crystals (MeOH–$CHCl_3$, 2 : 98); m.p. 198—199 °C; UV (MeOH) λ_{max} (log ε): 217 (3.18) nm; $[\alpha]_D^{20}$ +72.8 (*c* 0.060, MeOH); ECD (MeOH) λ_{max} ($\Delta\varepsilon$): 218 (+5.8), 245 (–4.0) nm; IR ν_{max}: 3523, 3436, 1766, 1736, 1661, 1445, 1380, 1105 cm^{-1}; ^1H and ^{13}C NMR data see Tables 1 and 4; (+)-HRESIMS *m/z* 509.2526 $[M + H]^+$ (calcd. for $C_{30}H_{37}O_7$, 509.2534).

Artemzhongdianolide B2 (2). White amorphous powder; $[\alpha]_D^{20}$ +71.3 (*c* 0.090, MeOH); UV (MeOH) λ_{max} (log ε): 217 (3.17) nm; ECD (MeOH) λ_{max} ($\Delta\varepsilon$): 220 (+7.2), 247 (–1.5) nm; IR ν_{max}: 3434, 1757, 1665, 1439, 1379, 1100 cm^{-1}; ^1H NMR and ^{13}C NMR data see Tables 1 and 4; (+)-HRESIMS *m/z* 509.2530 $[M + H]^+$ (calcd. for $C_{30}H_{37}O_7$, 509.2534).

Artemzhongdianolide B3 (3). Colorless orthorhombic crystals (MeOH–$CHCl_3$, 10 : 90); m.p. 201—202 °C; $[\alpha]_D^{20}$ –89.9 (*c* 0.095, MeOH); UV (MeOH) λ_{max} (log ε): 216 (3.37) nm; ECD (MeOH) λ_{max} ($\Delta\varepsilon$): 201 (+23.6), 231 (–12.8), 328 (–2.8) nm; IR ν_{max}: 3442, 1765, 1713, 1634, 1458, 1384, 1267, 1150 cm^{-1}; ^1H and ^{13}C NMR data see Tables 1 and 4; (–)-HRESIMS *m/z* 537.2499 $[M–H]^-$ (calcd. for $C_{31}H_{37}O_8$, 537.2494).

Artemzhongdianolide B4 (4). White amorphous powder; $[\alpha]_D^{20}$ +51.6 (*c* 0.060, MeOH); UV (MeOH) λ_{max} (log ε): 217 (3.08) nm; ECD (MeOH) λ_{max} ($\Delta\varepsilon$): 214 (+12.9), 247 (–8.8), 326 (+1.2) nm; IR ν_{max}: 3439, 1759, 1712, 1632, 1457, 1256, 1155, 1006 cm^{-1}; ^1H and ^{13}C NMR data see Tables 1 and 4; (–)-HRESIMS *m/z* 537.2497 $[M–H]^-$ (calcd. for $C_{31}H_{37}O_8$, 537.2494).

Artemzhongdianolide B5 (5). White amorphous powder; $[\alpha]_D^{20}$ –64.3 (*c* 0.047, MeOH); UV (MeOH) λ_{max} (log ε): 216 (3.18) nm; ECD (MeOH) λ_{max} ($\Delta\varepsilon$): 206 (+9.1), 229 (–4.2), 319 (–1.8) nm; IR ν_{max}: 3431, 1765, 1712, 1644, 1456, 1377, 1261, 1006 cm^{-1}; ^1H and ^{13}C NMR data see Tables 1 and 4; (+)-HRESIMS *m/z* 525.2492 $[M + H]^+$ (calcd. for $C_{30}H_{37}O_8$, 525.2483).

Artemzhongdianolide B6 (6). White amorphous powder; $[\alpha]_D^{20}$ –50.7 (*c* 0.078, MeOH); UV (MeOH) λ_{max} (log ε): 217 (3.35) nm; ECD (MeOH) λ_{max} ($\Delta\varepsilon$): 202 (+16.4), 230 (–5.3), 319 (–2.8) nm; IR ν_{max}: 3436, 1764, 1711, 1649, 1455, 1376, 1255, 1155 cm^{-1}; ^1H NMR and ^{13}C NMR data see Tables 1 and 4; (–)-HRESIMS *m/z* 523.2351 $[M–H]^-$ (calcd. for $C_{30}H_{35}O_8$, 523.2337).

Artemzhongdianolide B7 (7). Colorless orthorhombic crystals (MeOH–$CHCl_3$, 10 : 90); m.p. 200—201 °C; $[\alpha]_D^{20}$ –45.0 (*c* 0.055, MeOH); UV (MeOH) λ_{max} (log ε): 218 (3.28) nm; ECD (MeOH) λ_{max} ($\Delta\varepsilon$): 201 (+16.6), 231 (–2.6) nm; IR ν_{max}: 3443, 1765, 1717, 1638, 1457, 1384, 1255, 969, 947 cm^{-1}; ^1H and ^{13}C NMR data see Tables 2 and 4; (–)-HRESIMS *m/z* 601.2640 $[M + HCOO]^-$ (calcd. for $C_{32}H_{41}O_{11}$, 601.2654).

Artemzhongdianolide B8 (8). White amorphous powder; $[\alpha]_D^{20}$ +17.7 (*c* 0.060, MeOH); UV (MeOH) λ_{max} (log ε): 217 (2.70) nm; ECD (MeOH) λ_{max} ($\Delta\varepsilon$): 203 (+3.1), 231 (–0.9), 284 (+0.1) nm; IR ν_{max}: 3440, 1752, 1635, 1456, 1384, 1261, 1049, 949, 880 cm^{-1}; ^1H and ^{13}C NMR data see Tables 2 and 4; (–)-HRESIMS *m/z* 555.2608

$[M-H]^-$ (calcd. for $C_{31}H_{39}O_9$, 555.2600).

Artemzhongdianolide B9 (9). Colorless monoclinic crystals (MeOH–$CHCl_3$, 2 : 98); m.p. 204—205 °C; $[\alpha]_D^{20}$ +14.0 (*c* 0.050, MeOH); UV (MeOH) λ_{max} (log ε): 217 (3.10) nm; ECD (MeOH) λ_{max} ($\Delta\varepsilon$): 208 (+9.6), 242 (–4.1), 277 (–2.1) nm; IR ν_{max}: 3440, 1776, 1630, 1452, 1380, 1232, 1015 cm^{-1}; ^1H and ^{13}C NMR data see Tables 2 and 4; (+)-HRESIMS *m/z* 507.2365 $[M+H]^+$ (calcd. for $C_{30}H_{35}O_7$, 507.2377).

Artemzhongdianolide B10 (10). Colorless monoclinic crystals (MeOH–$CHCl_3$, 2 : 98); m.p. 204—205 °C; $[\alpha]_D^{20}$ –68.0 (*c* 0.080, MeOH); UV (MeOH) λ_{max} (log ε): 219 (3.14) nm; ECD (MeOH) λ_{max} ($\Delta\varepsilon$): 223 (–2.0), 280 (–1.8), 321 (–1.7) nm; IR ν_{max}: 3435, 1773, 1711, 1646, 1456, 1378, 1259, 1135, 1011 cm^{-1}; ^1H and ^{13}C NMR data see Tables 2 and 5; (+)-HRESIMS *m/z* 539.2272 $[M+H]^+$ (calcd. for $C_{30}H_{35}O_9$, 539.2276).

Artemzhongdianolide B11 (11). White amorphous powder; $[\alpha]_D^{20}$ +24.5 (*c* 0.060, MeOH); UV (MeOH) λ_{max} (log ε): 220 (2.74) nm; ECD (MeOH) λ_{max} ($\Delta\varepsilon$): 205 (+3.8), 224 (+1.4), 242 (–0.6), 279 (–0.3) nm; IR ν_{max}: 3440, 1778, 1633, 1456, 1384, 1235, 1164, 1023 cm^{-1}; ^1H and ^{13}C NMR data see Tables 2 and 5; (+)-HRESIMS *m/z* 541.2417 $[M+H]^+$ (calcd. for $C_{30}H_{37}O_9$, 541.2432).

Artemzhongdianolide B12 (12). White amorphous powder; $[\alpha]_D^{20}$ +75.2 (*c* 0.050, MeOH); UV (MeOH) λ_{max} (log ε): 220 (2.69) nm; ECD (MeOH) λ_{max} ($\Delta\varepsilon$): 203 (+16.7), 224 (+1.6), 242 (–3.0), 280 (–1.6) nm; IR ν_{max}: 3435, 1776, 1649, 1616, 1443, 1381, 1236, 1172 cm^{-1}; ^1H and ^{13}C NMR data see Tables 2 and 5; (+)-HRESIMS *m/z* 563.2245 $[M+Na]^+$ (calcd. for $C_{30}H_{36}O_9Na$, 563.2252).

Artemzhongdianolide B13 (13). Colorless orthorhombic crystals (MeOH–$CHCl_3$, 10 : 90); m.p. 204—205 °C; $[\alpha]_D^{20}$ +77.8 (*c* 0.060, MeOH); UV (MeOH) λ_{max} (log ε): 219 (2.98) nm; ECD (MeOH) λ_{max} ($\Delta\varepsilon$): 215 (+17.6) nm; IR ν_{max}: 3436, 1766, 1630, 1443, 1380, 1254, 1114, 1012 cm^{-1}; ^1H and ^{13}C NMR data see Tables 3 and 5; (+)-HRESIMS *m/z* 493.2566 $[M+H]^+$ (calcd. for $C_{30}H_{37}O_6$, 493.2585).

Artemzhongdianolide B14 (14). White amorphous powder; $[\alpha]_D^{20}$ +80.9 (*c* 0.040, MeOH); UV (MeOH) λ_{max} (log ε): 220 (3.30) nm; ECD (MeOH) λ_{max} ($\Delta\varepsilon$): 237 (+16.4), 322 (–1.8) nm; IR ν_{max}: 3434, 1766, 1711, 1652, 1446, 1384, 1257, 1111 cm^{-1}; ^1H NMR and ^{13}C NMR data see Tables 3 and 5; (–)-HRESIMS *m/z* 523.2352 $[M-H]^-$ (calcd. for $C_{30}H_{35}O_8$, 523.2337).

Artemzhongdianolide B15 (15). White amorphous powder; $[\alpha]_D^{20}$ +53.9 (*c* 0.046, MeOH); UV (MeOH) λ_{max} (log ε): 251 (2.94) nm; ECD (MeOH) λ_{max} ($\Delta\varepsilon$): 201 (–4.4), 217 (+9.8) nm; IR ν_{max}: 3446, 1771, 1688, 1638, 1619, 1456, 1380, 1257, 1143, 1009 cm^{-1}; ^1H and ^{13}C NMR data see Tables 3 and 5; (–)-HRESIMS *m/z* 535.2344 $[M+HCOO]^-$ (calcd. for $C_{31}H_{35}O_8$, 535.2337).

Artemzhongdianolide B16 (16). White amorphous powder; $[\alpha]_D^{20}$ +99.0 (*c* 0.040, MeOH); UV (MeOH) λ_{max} (log ε): 220 (3.11) nm; ECD (MeOH) λ_{max} ($\Delta\varepsilon$): 217 (+10.7), 295 (+0.6) nm; IR ν_{max}: 3438, 1772, 1716, 1634, 1448, 1381, 1242, 1112 cm^{-1}; ^1H and ^{13}C NMR data see Tables 3 and 5; (+)-HRESIMS *m/z* 491.2435 $[M+H]^+$ (calcd. for $C_{30}H_{35}O_6$, 491.2428).

Artemzhongdianolide B17 (17). White amorphous powder; $[\alpha]_D^{20}$ +26.9 (*c* 0.075, MeOH); UV (MeOH) λ_{max} (log ε): 220 (2.88) nm; ECD (MeOH) λ_{max} ($\Delta\varepsilon$): 216 (+8.6), 250 (–0.5) nm; IR ν_{max}: 3434, 1767, 1736, 1631, 1449, 1382, 1256, 1142, 1008 cm^{-1}; ^1H NMR and ^{13}C NMR data see Tables 3 and 5; (–)-HRESIMS *m/z* 571.2561 $[M+HCOO]^-$ (calcd. for $C_{31}H_{39}O_{10}$, 571.2549).

X-ray crystallographic analysis and ECD calculations

See the Supporting Information.

Cell lines and cell culture

HepG2, Huh7 and SK-Hep-1 cell lines were purchased from Shanghai Jining Biotechnology Co., Ltd. (Shanghai, China) and maintained in a humidified atmosphere at 37 °C and 5% CO_2.

Western blot

The expression of apoptosis and cell cycle related proteins, p38 and p-p38 proteins were determined by Western blot. Primary antibodies used in this study were listed as follows: anti-β-actin (66009-1-Ig), anti-Cyclin D1(60186-1-Ig) were obtained from Protintech Group; anti-Bax (ab32503), anti-Bcl-2 (ab182858) were obtained from Abcam (Cambridge, MA, United States); anti-p21 (2947), anti-CDK4 (12790), anti-CDK6 (13331), anti-p38 (8690), anti-Phospho-p38 MAPK (4522) were obtained from Cell Signaling Technology (Danvers, MA, United States). Secondary anti-rabbit antibody (SA00001-2) and anti-mouse antibody (SA00001-1) were obtained from Protintech Group. Briefly, HepG2 cells were seeded into 6-well plates and treated with compound **9**. The cells were collected and lysed in RIPA buffer to extract total protein, and the protein concentration was determined by the BCA method.[26] Samples were then fractionated using SDS-PAGE and transferred to PVDF membranes. Then, the membranes were incubated with specific primary antibodies at 4 °C overnight. The secondary antibody was incubated for 2 h at room temperature. Proteins were detected by ECL solution (Advansta, USA) and photographed by a multispectral imaging system (UVP, USA).

Method for prediction of target proteins

To predict the target proteins for artemzhongdianolide B9, a machine learning method was introduced, which is based on the assumption that compounds with similar chemical structure will implement similar function by binding same or functional related proteins. To this end, the known 11 416 drug-target interactions were collected from DrugBank[27] as the gold-standard data to learn the underlying rule that compounds with what types of structures could bind the proteins with certain type of pocket structures. Specifically, the compounds were represented by the chemical molecular descriptors (QuaSAR-Descriptor in the Molecular Operating Environment (MOE)) based on their chemical structures, and target proteins were represented by their amino acid sequences. Tanimoto coefficients[28] were introduced to calculate the similarities among compounds. The similarity between compound A and compound B was calculated as follows:

$$sim(d_A, d_B) = \frac{x_A^T x_B}{x_A^T x_A + x_B^T x_B - x_A^T x_B}$$

where x_A, x_B are the chemical molecular descriptors for drug A and drug B, respectively. The exponential function was adopted to transform the genetic distances to the protein similarities. The similarity between protein M and protein N was calculated by the following equation:

$$sim(p_M, p_N) = \exp\left(-dist(p_M, p_N)\right)$$

where, $dist(p_M, p_N)$ is genetic distance between protein M and protein N, which was calculated via "seqinr" R package. The random forest classifier[29] was introduced as the machine learning algorithm to train the protein target predictor. The randomly selected drug and protein pairs that were not shown in training positive data were used as the training negatives. The training negative data has the same scale as the training positive data did. Finally, the potential protein targets were predicted *via* above constructed predictor. The random forest algorithm was implemented *via* "randomForest" R package with default parameters.

Supporting Information

The supporting information for this article is available on the WWW under https://doi.org/10.1002/cjoc.202300166.

Acknowledgement

This work was supported by the Key Program of National Natural Science Foundation of China (22137008) and the Xingdian Yingcai Project (YNWR-KJLJ-2019-002), the Youth Innovation Promotion Association, CAS (2020386), the Reserve Talents of Young

and Middle-aged Academic and Technical Leaders in Yunnan Province (202105AC160021).

References

[1] Forner, A.; Reig, M.; Bruix, J. Hepatocellular carcinoma. *Lancet* **2018**, *391*, 1301–1314.

[2] Liu, S.; Qiu, J.; He, W.; Geng, C.; He, G.; Liu, C.; Cai, D.; Liu, X.; Tian, B.; Pan, H. TUG1 long non-coding RNA enlists the USF1 transcription factor to overexpress ROMO1 leading to hepatocellular carcinoma growth and metastasis. *MedComm* **2020**, *1*, 386–399.

[3] Yarchoan, M.; Agarwal, P.; Villanueva, A.; Rao, S.; Dawson, L. A.; Karasic, T.; Llovet, J. M.; Finn, R. S.; Groopman, J. D.; El-Serag, H. B.; Monga, S. P.; Wang, X. W.; Karin, M.; Schwartz, R. E.; Tanabe, K. K.; Roberts, L. R.; Gunaratne, P. H.; Tsung, A.; Brown, K. A.; Lawrence, T. S.; Salem, R.; Singal, A. G.; Kim, A. K.; Rabiee, A.; Resar, L.; Meyer, J.; Hoshida, Y.; He, A. R.; Ghoshal, K.; Ryan, P. B.; Jaffee, E. M.; Guha, C.; Mishra, L.; Coleman, C. N.; Ahmed, M. M. Recent developments and therapeutic strategies against hepatocellular carcinoma. *Cancer Res.* **2019**, *79*, 4326–4330.

[4] Liang, L.; Liu, Y.; Kang, B.; Wang, R.; Sun, M.-Y.; Wu, Q.; Meng, X.-F.; Lin, J.-P. Large-scale comparison of machine learning algorithms for target prediction of natural products. *Brief. Bioinform.* **2022**, *23*, bbac359.

[5] Su, L.-H.; Zhang, X.-T; Ma, Y.-B.; Geng, C.-A.; Huang, X.-Y.; Hu, J.; Li, T.-Z.; Tang, S.; Shen, C.; Gao, Z.; Zhang, X.-M.; Chen, J.-J. New guaiane-type sesquiterpenoid dimers from *Artemisia atrovirens* and their antihepatoma activity. *Acta Pharm. Sin. B* **2021**, *11*, 1648–1666.

[6] Shang, C.; Huang, X.-Y.; Wang, Y.; Dong, W.; He, X.-F.; Li, T.-Z.; Chen, J.-J. Artemongolides A–F, undescribed sesquiterpenoid dimers from *Artemisia mongolica* and their antihepatic fibrosis activities. *Org. Biomol. Chem.* **2023**, *21*, 823–831.

[7] Lee, S.-H.; Kang, H.-M.; Song, H.-C.; Lee, H.; Lee, U. C.; Son, K.-H.; Kim, S.-H.; Kwon, B.-M. Sesquiterpene lactones, inhibitors of farnesyl protein transferase, isolated from the flower of *Artemisia sylvatica*. *Tetrahedron* **2000**, *56*, 4711–4715.

[8] Xue, G.-M.; Han, C.; Chen, C.; Li, L.-N.; Wang, X.-B.; Yang, M.-H.; Gu, Y.-C.; Luo, J.-G.; Kong, L.-Y. Artemisians A–D, diseco-guaianolide involved heterodimeric [4 + 2] adducts from *Artemisia argyi*. *Org. Lett.* **2017**, *19*, 5410–5413.

[9] Bonney, E. A. Mapping out p38MAPK. *Am. J. Reprod. Immunol.* **2017**, *77*, e12652.

[10] Iyoda, K.; Sasaki, Y.; Horimoto, M.; Toyama, T.; Yakushijin, T.; Sakakibara, M.; Takehara, T.; Fujimoto, J.; Hori, M.; Wands, J. R.; Hayashi, N. Involvement of the p38 mitogen-activated protein kinase cascade in hepatocellular carcinoma. *Cancer* **2003**, *97*, 3017–3026.

[11] Li, L.; Zheng, B.-B.; Ma, L.-D.; Sun, X.; Chang, J.-J.; Xie, W.-D.; Li, X. Telekin suppresses human hepatocellular carcinoma cells in vitro by inducing G2/M phase arrest *via* the p38 MAPK signaling pathway. *Acta Pharmacol. Sin.* **2014**, *35*, 1311–1322.

[12] Rudalska, R.; Dauch, D.; Longerich, T.; McJunkin, K.; Wuestefeld, T.; Kang, T.-W.; Hohmeyer, A.; Pesic, M.; Leibold, J.; von Thun, A.; Schirmacher, P.; Zuber, J.; Weiss, K.-H.; Powers, S.; Malek, N. P.; Eilers, M.; Sipos, B.; Lowe, S. W.; Geffers, R.; Laufer, S.; Zender, L. In vivo RNAi screening identifies a mechanism of sorafenib resistance in liver cancer. *Nat. Med.* **2014**, *20*, 1138–1146.

[13] Prihoda, D.; Maritz, J. M.; Klempir, O.; Dzamba, D.; Woelk, C. H.; Hazuda, D. J.; Bitton, D. A.; Hannigan, G. D. The application potential of machine learning and genomics for understanding natural product diversity, chemistry, and therapeutic translatability. *Nat. Prod. Rep.* **2021**, *38*, 1100–1108.

[14] He, X.-F.; Ma, W.-J.; Hu, J.; Li, T.-Z.; Geng, C.-A.; Ma, Y.-B.; Wang, M.-F.; Yang, K.-X.; Zhang, X.-M.; Chen, J.-J. Diverse structures and antihepatoma effect of sesquiterpenoid dimers from Artemisia eriopoda by AKT/STAT signaling pathway. *Sig. Transduct Target Ther.* **2023**, *8*, 64.

[15] Gao, Z.; Ma, W.-J.; Li, T.-Z.; Ma, Y.-B.; Hu, J.; Huang, X.-Y.; Geng, C.-A.; He, X.-F.; Zhang, X.-M.; Chen, J.-J. Artemidubolides A–T, cytotoxic unreported guaiane-type sesquiterpenoid dimers against three hepatoma cell lines from *Artemisia dubia*. *Phytochemistry* **2022**, *202*, 113299.

[16] He, X.-F.; Li, Q.-H.; Li, T.-Z.; Ma, Y.-B.; Dong, W.; Yang, K.-X.; Geng, C.-A.; Zhang, H.-W.; Wang, W.; Chen, J.-J. Artemeriopolides A–D, two types of sesquiterpenoid dimers with rare carbon skeletons from *Artemisia eriopoda* and their antihepatoma cytotoxicity. *Org. Chem. Front.* **2023**, https://doi.org/10.1039/D3QO00223C.

[17] Su, L.-H.; Li, T.-Z.; Ma, Y.-B.; Geng, C.-A.; Huang, X.-Y.; Zhang, X.; Gao, Z.; Chen, J.-J. Artematrovirenolides A—D and artematrolides S—Z, sesquiterpenoid dimers with cytotoxicity against three hepatoma cell lines from *Artemisia atrovirens*. *Chin. J. Chem.* **2022**, *40*, 104–114.

[18] Su, L.-H.; Li, T.-Z.; Geng, C.-A.; Ma, Y.-B.; Huang, X.-Y.; Wang, J.-P.; Zhang, X.-M.; Chen, J.-J. Trimeric and dimeric sesquiterpenoids from *Artemisia atrovirens* and their cytotoxicities. *Org. Chem. Front.* **2021**, *8*, 1249–1256.

[19] Su, L.-H.; Ma, W.-J.; Ma, Y.-B.; Li, T.-Z.; Geng, C.-A.; Dong, W.; He, X.-F.; Chen, J.-J. Artemiprinolides A–M, thirteen undescribed sesquiterpenoid dimers from *Artemisia princeps* and their antihepatoma activity. *Phytochemistry* **2023**, *211*, 113714.

[20] Li, T.-Z.; Yang, X.-T.; Wang, J.-P.; Geng, C.-A.; Ma, Y.-B.; Su, L.-H.; Zhang, X.-M.; Chen, J.-J. Biomimetic synthesis of lavandiolides H, I, and K and artematrolide F *via* Diels–Alder reaction. *Org. Lett.* **2021**, *23*, 8380–8384.

[21] Dong, W.; Li, T.-Z.; Huang, X.-Y.; He, X.-F.; Geng, C.-A.; Zhang, X.-M.; Chen, J.-J. Artemzhongdianolides A1-A21, antihepatic fibrosis guaiane-type sesquiterpenoid dimers from *Artemisia zhongdianensis*. *Bioorg. Chem.* **2022**, *128*, 106056.

[22] Oikawa, H.; Tokiwano, T. Enzymatic catalysis of the Diels–Alder reaction in the biosynthesis of natural products. *Nat. Prod. Rep.* **2004**, *21*, 321–352.

[23] Wang, S.; Sun, J.; Zeng, K.; Chen, X.; Zhou, W.; Zhang, C.; Jin, H.; Jiang, Y.; Tu, P. Sesquiterpenes from *Artemisia argyi*: absolute configurations and biological activities. *Eur. J. Org. Chem.* **2014**, *2014*, 973–983.

[24] Wagner, E. F.; Nebreda, Á. R. Signal integration by JNK and p38 MAPK pathways in cancer development. *Nat. Rev. Cancer* **2009**, *9*, 537–549.

[25] Hui, L.; Bakiri, L.; Mairhorfer, A.; Schweifer, N.; Haslinger, C.; Kenner, L.; Komnenovic, V.; Scheuch, H.; Beug, H.; Wagner, E. F. p38α suppresses normal and cancer cell proliferation by antagonizing the JNK–c-Jun pathway. *Nat. Genet.* **2007**, *39*, 741–749.

[26] Liu, M.-J.; Yue, P. Y.-K.; Wang, Z.; Wong, R. N.-S. Methyl protodioscin induces G2/M arrest and apoptosis in K562 cells with the hyperpolarization of mitochondria. *Cancer Lett.* **2005**, *224*, 229–241.

[27] Wishart, D. S.; Knox, C.; Guo, A. C.; Shrivastava, S.; Hassanali, M.; Stothard, P.; Chang, Z.; Woolsey, J. DrugBank: a comprehensive resource for in silico drug discovery and exploration. *Nucleic Acids Res.* **2006**, *34*, D668–D672.

[28] Bajusz, D.; Rácz, A.; Héberger, K. Why is Tanimoto index an appropriate choice for fingerprint-based similarity calculations? *J. Cheminf.* **2015**, *7*, 20.

[29] Breiman, L. Random Forests. *Mach. Learn.* **2001**, *45*, 5–32.

Manuscript received: March 23, 2023
Manuscript revised: May 13, 2023
Manuscript accepted: May 14, 2023
Accepted manuscript online: May 20, 2023
Version of record online: June 24, 2023

The Authors

Left to Right: Wei Dong, Wen-Jing Ma, Yun-Bao Ma, Feng-Jiao Li, Tian-Ze Li, Yong-Cui Wang, Xiao-Feng He, Chang-An Geng, Xue-Mei Zhang, Ji-Jun Chen